Scientific African 31 (2026) e03136

Contents lists available at ScienceDirect

Scientific African

journal homepage: www.elsevier.com/locate/sciaf

Comparative study of biogenic iron oxide nanoparticles from various extracts of Punica granatum and their efficient application for removal of BTEX

Ngozi Enemuo [a], Michael O. Daramola [b], Heidi Richards [a,*]

[a] Molecular Sciences Institute, School of Chemistry, University of the Witwatersrand, Private Bag X3, WITS, 2050 Johannesburg, South Africa
[b] Sustainable Energy and Environment Research Group (SEERG), Department of Chemical Engineering, Faculty of Engineering, Built Environment and Information Technology, University of Pretoria, Hatfield, 0028, Pretoria, South Africa

ARTICLE INFO

Editor: Mohamed Fathy El-Amin Mousa.

Keywords:
Iron oxide nanoparticles
Phytochemicals
Plant extracts
Water treatment
Adsorption

ABSTRACT

This study investigated the potential of Punica granatum-mediated iron oxide nanoparticles (FeNPs) in the adsorptive removal of BTEX from wastewater. To gain insight into achieving optimum BTEX removal, the study highlighted the role of phytochemical composition in determining the features of the resulting nanoparticles and, subsequently, the FeNPs' adsorption capacity. It established the Punica granatum part that generates ideal FeNPs with optimum performance in BTEX adsorption. Three Punica granatum parts, the leaves, peels, and seeds, were utilized for the biogenic synthesis of the FeNPs, and the features and performance of the FeNPs in BTEX adsorptive removal were analyzed. It was found that the FeNPs from various Punica granatum parts, namely FeNPs-leaves, FeNPs-peels, and FeNPs-seeds, exhibited distinct features due to the unique phytochemical composition of these parts, as indicated by their total phenolic content (TPC) measurement and GC–MS analysis. The XRD result showed that bio-reduction using the leaves extract yielded magnetite, while bluish-black maghemite and yellowish-brown maghemite were obtained from the peels and seeds extracts, respectively. The three FeNPs also have different specific surface areas, at 8.61 m^2/g, 48.45 m^2/g, and 35.40 m^2/g for FeNPs-leaves, FeNPs-peels, and FeNPs-seeds, respectively. The properties of the FeNPs influenced their BTEX adsorption capacity, with the FeNPs-peels (48.45 m^2/g) and FeNPs-seeds (35.40 m^2/g) exhibiting higher specific surface area than the FeNPs-leaves (8.61 m^2/g), which reflected in the higher BTEX adsorption capacity obtained for the FeNPs-peels and FeNPs-seeds. The BTEX adsorption on the FeNPs mainly occurs through chemisorption in a monolayer surface, as indicated by the adsorption data fitting in pseudo-second-order and the Langmuir isotherm model.

Introduction

Benzene, toluene, ethylbenzene, and xylene, collectively termed BTEX, are toxic aromatic hydrocarbons commonly found in industrial wastewater, especially petroleum-based wastewater [1]. The release of poorly treated or untreated BTEX-contaminated wastewater into the environment is a major environmental and health risk due to their persistence, volatility, and toxicity [2,3]. In aquatic systems, BTEX compounds reduce dissolved oxygen levels and bioaccumulate in organisms, leading to metabolic disruption

* Corresponding author at: 1 Jan Smuts Ave, Braamfontein, Johannesburg, Private Bag 3, Wits, 2050, South Africa.
E-mail address: heidi.richards@wits.ac.za (H. Richards).

https://doi.org/10.1016/j.sciaf.2025.e03136
Received 11 August 2025; Received in revised form 3 November 2025; Accepted 12 December 2025
Available online 14 December 2025

and mortality [4]. In soils, they impair microbial activity and can leach into groundwater, rendering it unsafe for consumption [1]. Moreover, volatilized BTEX contributes to air pollution and the formation of photochemical smog [2,5]. Prolonged human exposure to BTEX-contaminated water or air can cause neurological damage, organ dysfunction, and cancer, with benzene identified as a potent human carcinogen [1,4]. Hence, devising an effective and efficient treatment approach for BTEX wastewater is critical.

Various methods have been used to remove BTEX compounds from wastewater, including biological degradation, advanced oxidation processes (AOPs), and membrane filtration [3,6,7]. However, each of these techniques has downsides that limit their application for BTEX removal. Biological treatment is environmentally friendly, but often inefficient at removing BTEX due to microbial inhibition [8]. AOPs can effectively degrade BTEX into less harmful compounds, but require high energy input and often use expensive, and usually toxic oxidants [7]. Membrane filtration provides physical separation of BTEX, but can be affected by severe fouling that negatively impacts the membrane integrity [9]. Among these methods, adsorption of BTEX using nanomaterials has gained significant attention due to its simplicity, cost-effectiveness, and high removal efficiency [2]. Advancements in nanotechnology have introduced eco-friendly synthesis routes that minimize the use of hazardous reagents and energy consumption, thereby promoting the development of green nanomaterials for safer, more sustainable environmental remediation [10]. Among these green approaches, the biogenic synthesis of nanomaterials using plant extracts has gained prominence due to its sustainability, simplicity, and low environmental impact. Compared with conventional chemical and physical synthesis methods, biogenic routes eliminate the need for harsh chemicals, reduce waste generation, and utilize naturally occurring phytochemicals as reducing and stabilizing agents [11]. This not only makes the process safer and more cost-effective but also produces nanomaterials with enhanced surface reactivity, making them highly suitable for environmentally benign BTEX adsorption.

For the use of plant substrates in nanomaterials synthesis, the type and composition of the plants' phytochemicals directly affect the properties of the nanomaterials and, subsequently, their performance in wastewater treatment [12–14]. Thus, research efforts are increasingly advancing toward understanding the correlation between a plant's phytochemical composition and the properties and performance of resulting nanomaterials. Liu et al. [15] studied and compared the role of the phytochemicals of the leaf extracts of three plants, Eriobotrya japonica (EJ), Populus (PL), and Cupressus *funebris* (CF) on the properties of biogenic synthesized Ag nanoparticles (AgNPs), and the subsequent performance of the AgNPs in the degradation of various organic dyes from dyeing wastewater. They found that the EJ extract has a higher capability to act as a reducing and stabilizing agent in the biogenic synthesis of the AgNPs, and the resulting AgNPs from the EJ extract have better catalytic and antibacterial performance than the AgNPs from the other studied extracts. In another study, Bopape et al. [16] studied the effect of the concentration of the extract of the C. *benghalensis* plant on the morphology of the synthesized ZnO-NPs, and the efficiency of the ZnO-NPs to photodegrade methylene blue (MB) dye. The study reported that the morphology of the ZnO-NPs was impacted by the plant extract concentrations, with the lower plant concentration producing platelets-shaped ZnO-NPs. At the same time, spherical ZnO-NPs were obtained from higher plant extract concentrations, which also exhibited higher photodegradation of MB in the wastewater. This variation in the property and performance of the biogenic synthesized ZnO-NPs was linked to the amount of phytochemicals in the different prepared plant extracts. Another similar study investigated the variations in the phytochemical composition of *H. perforatum* plant extract during the biogenic synthesis of AgNPs to establish the role of the plant's phytochemicals in the synthetic procedure [12]. The study identified the phenolic acids and flavonoids of the plant extracts as reducing agents, while xanthones and phloroglucinols are the capping agents.

Punica granatum plant is particularly suited for plant-based nanomaterial synthesis due to its robust phytochemical profile and ease of cultivation. The plant's parts are rich in polyphenols, flavonoids, and tannins, which serve as natural reducing and stabilizing agents, enabling the eco-friendly formation of nanoparticles under mild conditions [17,18]. In addition, it is very adaptable to a wide range of soils, highly tolerant of drought, and grows in various climatic conditions, ensuring consistent biomass production and making it a sustainable, readily available source for green synthesis [19].

Motivated by the lack of studies on the use of biogenic synthesized FeNPs, particularly Punica granatum-mediated FeNPs, for the adsorptive removal of BTEX, this work investigated the properties of FeNPs from the Punica granatum leaves, peels, and seeds and their subsequent application in BTEX wastewater treatment. This aimed to identify the part of Punica granatum that produces FeNPs with ideal features, resulting in optimal performance in the adsorptive removal of BTEX from wastewater, since the composition of the phytochemicals in these Punica granatum parts varies [18]. Hence, an investigation into the part of the Punica granatum that produces the prime FeNPs features due to its unique phytochemical composition is paramount for developing ideal FeNPs for BTEX wastewater treatment. The study investigated an effective method for addressing BTEX contamination in our water bodies using Punica granatum-mediated FeNPs. This study further evaluated the adsorption kinetics and isotherm profile of the FeNPs in BTEX removal to gain insight into the nature of BTEX adsorption using the biogenic synthesized FeNPs. It is essential to note that utilizing the three parts of the Punica granatum in this study is considered sustainable in terms of food conservation, as the Punica granatum fruit peels and seeds are food waste, while the leaves are not edible.

Materials and methods

Materials

The Punica granatum's leaves, peels, and seeds were harvested from the Punica granatum plant located at the School of Chemical and Metallurgical Engineering, Wits University, Braamfontein. Folin-ciocalteu reagent, gallic acid, sodium carbonate, benzene (99.8 %), toluene (99.9 %), xylene (≥99 %), ethylbenzene (>99.9 %), and Iron (III) chloride, were acquired from Sigma Aldrich. The deionized water (DI water; 18.2 MΩcm @25 °C) utilized in this work was obtained from the Direct-Q UV millipore water purification unit. The chemicals were utilized as they were received without further purification.

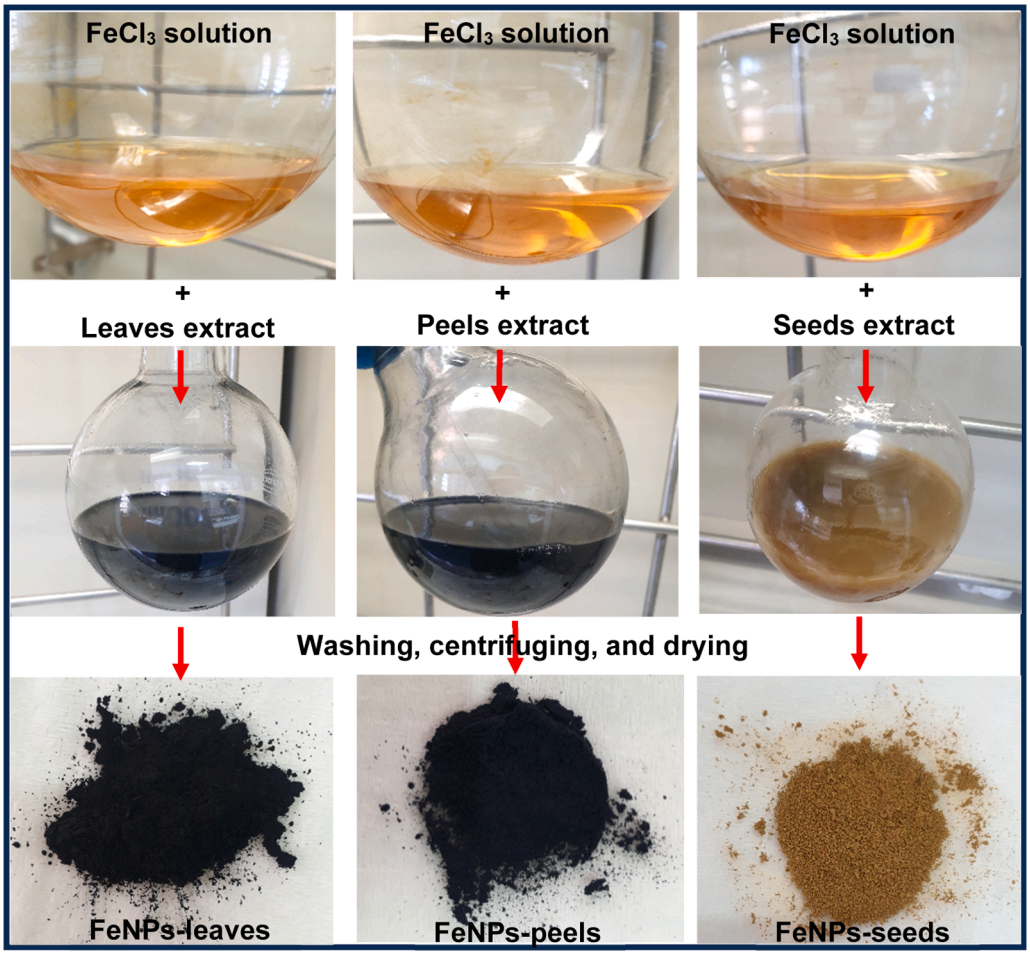

Fig. 1. The experimental procedure for the synthesis of the iron oxide NPs.

Preparation of the extracts of the Punica granatum

The peels and seeds were obtained from the Punica granatum fruits by separating these parts from the fruit, while the leaves were directly plucked from the tree. All the parts (leaves, seeds, and peels) were well rinsed with tap water to wash off the dust or impurities and then left to dry in a clean, open space. Afterward, the parts were additionally oven-dried at 50 °C for 3 days to obtain well-dried Punica granatum leaves, peels, and seeds. The dried parts were separately ground into fine powders using a clean grinder. The aqueous extracts of the parts were then obtained by mixing 20 g of each powder separately with DI water (200 mL) and shaking the mixture at 150 rpm for 8 h, which is then sonicated for 30 min. The mixtures were then initially filtered using a stainless steel sieve, followed by vacuum filtration with a Whatman filter no. 1. The obtained separate extract of the Punica granatum leaves, peels, and seeds were stored at 4 °C and employed for the biogenic synthesis of the iron oxide nanoparticles (FeNPs).

Synthesis of the iron oxide NPs

The FeNPs were biogenically synthesized using the various prepared Punica granatum extracts to reduce the iron precursor, $FeCl_3$. Three iron oxide NPs were obtained by utilizing either the leaves, peels, and seeds extracts to reduce the precursor according to the procedure described below:

$FeCl_3$ solution was first obtained by dissolving 1.2 g of $FeCl_3$ in DI water (70 mL) with continuous stirring. 140 mL of the Punica granatum extract was gently poured into the $FeCl_3$ solution and stirred continuously for 3 h at 80 °C. At this stage, the reaction mixtures containing the peels and leaves extract changed from the initial yellow colour to black. This indicates the complete reduction of the $FeCl_3$ precursor to the iron oxide NPs, as shown in Fig. 1. There was no significant colour change in the reaction mixture containing the seeds extract after 3 h; hence its reaction time was extended. After 8 h, the colour of the reaction mixture containing the seeds extract changed to yellowish-brown, as also shown in Fig. 1. Then, the three reaction mixtures were left to cool and then centrifuged to recover the NPs. The NPs were thoroughly washed thrice with ethanol and DI water by shaking the NPs suspension for 15 min and sonicating for 10 min to remove impurities. The sonication of the NPs also ensures the breakdown of the clusters of the NPs into individual NPs.

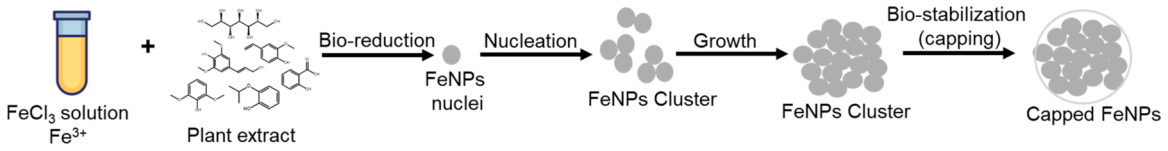

Fig. 2. The mechanism of the biosynthesis of the FeNPs using the Punica granatum extracts.

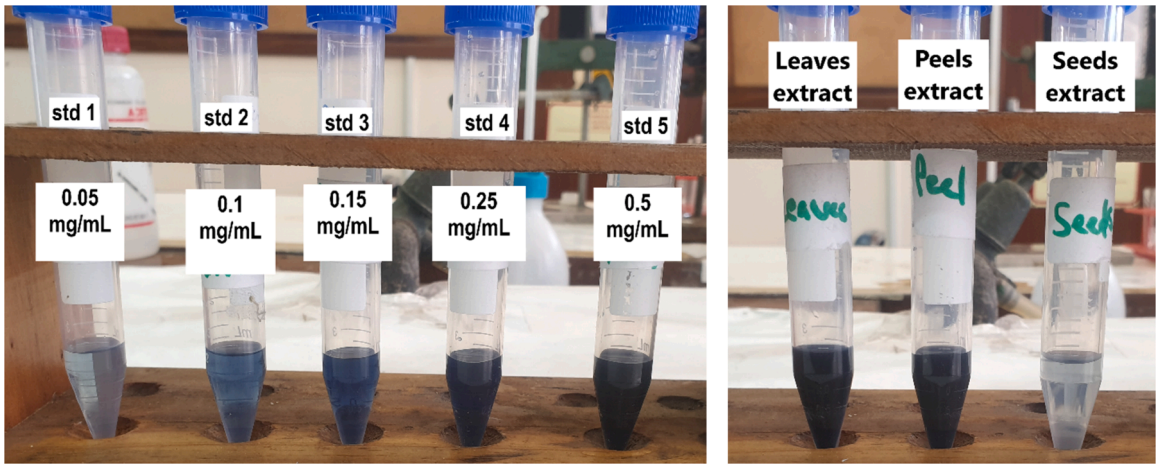

Fig. 3. The prepared standards and Punica granatum extracts for total phenolic content measurements.

Lastly, the resulting NPs were oven-dried at 50 °C for 3 h to obtain the NPs in dry form, which was crushed with mortar and pestle into fine NP powder. The NPs were then stored in an airtight container and used for the related characterizations and performance analysis in this study.

The mechanism of the biosynthesis is represented in Fig. 2. The phytochemicals in the plant extract consist of compounds with electron-donating functional groups such as -OH, -C=O, and -NH_2 (as depicted in the FTIR result), which reduce the Fe^{3+} to the FeNPs nuclei (Fe_3O4 or Fe_2O_3). This is followed by the nucleation step, which involves the initial formation of small FeNPs clusters and the subsequent growth of these clusters into larger FeNPs. The active phytochemicals in the plant extract also cap the formed FeNPs cluster, controlling the particle size.

Characterization of the Punica granatum extracts and iron oxide NPs

The total phenolic content (TPC) of the various Punica granatum extracts was calculated according to the Folin-Ciocalteu assay [20], with few modifications such as the volume of the Folin-Ciocalteu reagent used, the volume of the extract used, and the Na_2CO_3 concentration. The Folin-Ciocalteu reagent (1 mL) was diluted with DI water (9 mL). Na_2CO_3 solution was made by dissolving 7.5 g of Na_2CO_3 in DI water (100 mL) to obtain 7.5 % (w/v) Na_2CO_3 solution. This is followed by the well mixing of 200 μL of each prepared extract (10 mg/mL) with 1.0 mL of the diluted Folin-Ciocalteu reagent; then the mixture was kept in a dark cabinet for 5 min. Afterward, 0.8 mL of the prepared Na_2CO_3 was added to the mixture, thoroughly mixed for 1 min using a velp scientifica vortex mixer, and left to stand in a dark cabinet for 2 h. The resulting mixtures are shown in Fig. 3. Gallic acid was the standard compound used in the TPC measurement, and the gallic acid stock solution was prepared by thoroughly dissolving 0.5 g of gallic acid in 100 mL of DI water to obtain a 5 mg/mL stock solution. The standard amounts (0.05, 0.1, 0.15, 0.25, and 0.5 mg/mL) were prepared by taking aliquots of the gallic acid stock solution and diluting accordingly, and 1 mL of the diluted Folin-Ciocalteu reagent and 0.8 mL of the prepared Na_2CO_3 were added to each of the standards. The standards were kept in a dark cabinet for 2 h, and the resulting standards are shown in Fig. 3 The absorbance of the standards and Punica granatum extracts at 765 nm was measured against a blank using an Agilent Cary Series UV–Vis Spectrophotometer. The measurements were all done in triplicates, with the TPC quoted as mg gallic acid equivalents (GAE) per g of either the dry leaves, peels, or seeds, which was calculated using Eq. (1).

$$C = cV/M \tag{1}$$

with C denoting the total phenolic content (mg GAE/g of dry plant). c, V, and M are the gallic acid concentration obtained from the calibration curve (mg/mL), the various extract volume (mL), and mass of the dry plant (g), respectively.

The phytochemicals in the Punica granatum extracts were determined with an Agilent GC 7890B, having a 30 m × 0.25 mm ID × 0.25 μm Rxi-5Sil MS capillary column, coupled to a Gerstel MultiPurpose Sampler robotic series and a LECO Pegasus 4D GC×GC-Time-of-Flight Mass Spectrometer (TOFMS). A 0.45 μm polytetrafluoroethylene (PTFE) filter was used to filter the Punica granatum extracts

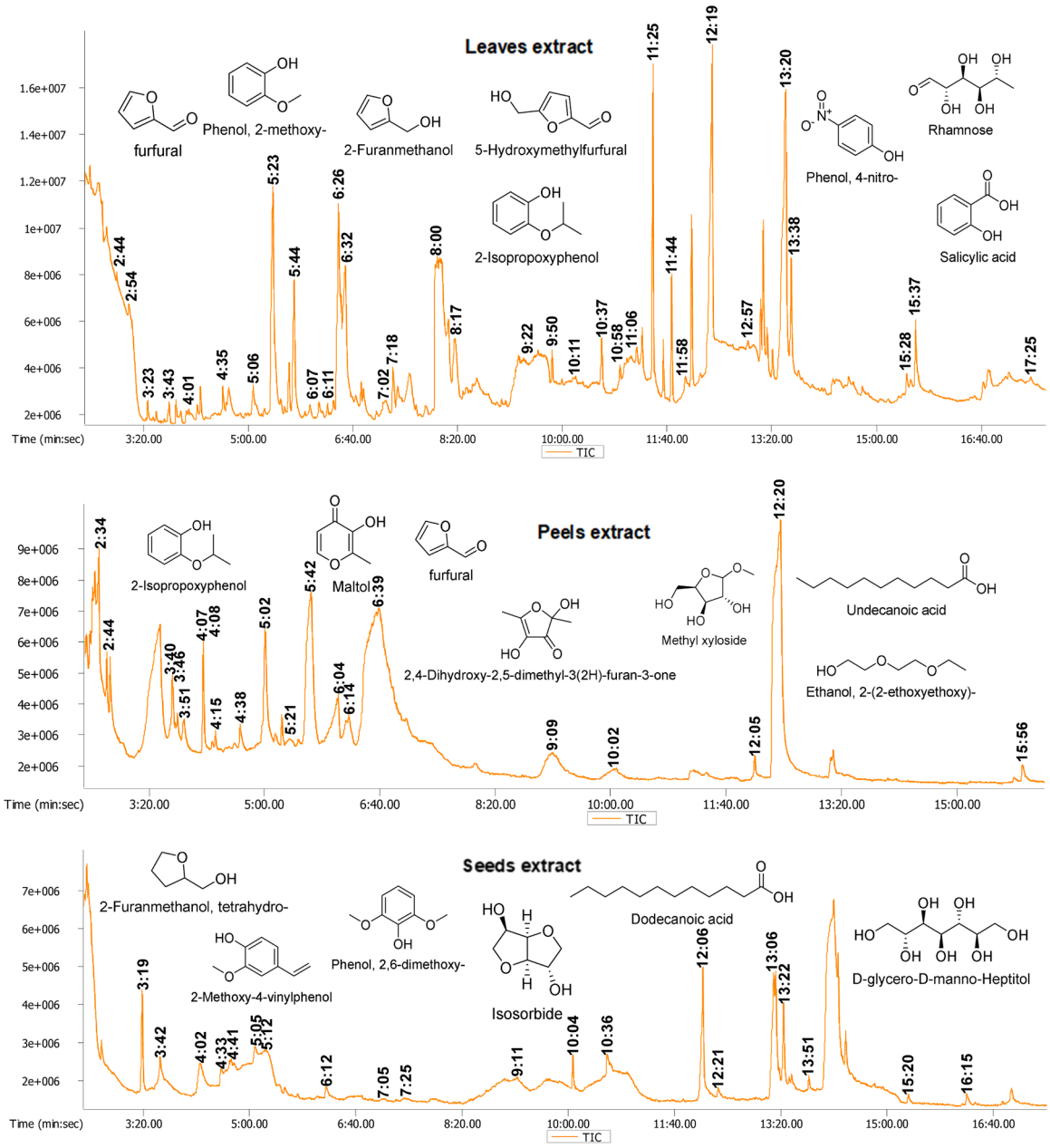

Fig. 4. GC–MS chromatograms of the Punica granatum leaves, peels, and seeds extracts.

before the analysis, and a 1 μL injection volume (splitless mode) was set, with helium mobile phase. Programming of the temperature gradient of the oven was thus: 50 °C for 30 sec, followed by 300 °C for 2 min at 15 °C/min. The National Institute Standard and Technology (NIST) database was used to interpret the GC–MS spectra and to match the phytochemicals found in the extracts.

Some of the Punica granatum extracts were lyophilized with an Alpha 1–2 LDplus freeze-dryer, and the functional groups in the lyophilized extracts were assessed using Bruker Tensor 27 FT-IR spectrometer.

The FeNPs were identified by XRD performed on a Bruker benchtop D2 phaser. A high-resolution Carl Zeiss SEM and JEOL JEM-2100F TEM were utilized to ascertain the NPs' shape and size respectively. Micrometrics TriStar II Plus version 3.03 was utilized to determine the NPs' textural property via N_2 physio-sorption at 77k. The NPs' surface charge was obtained by measuring their zeta potential, which was done on a Malvern Zetasizer Nano ZS Instrument.

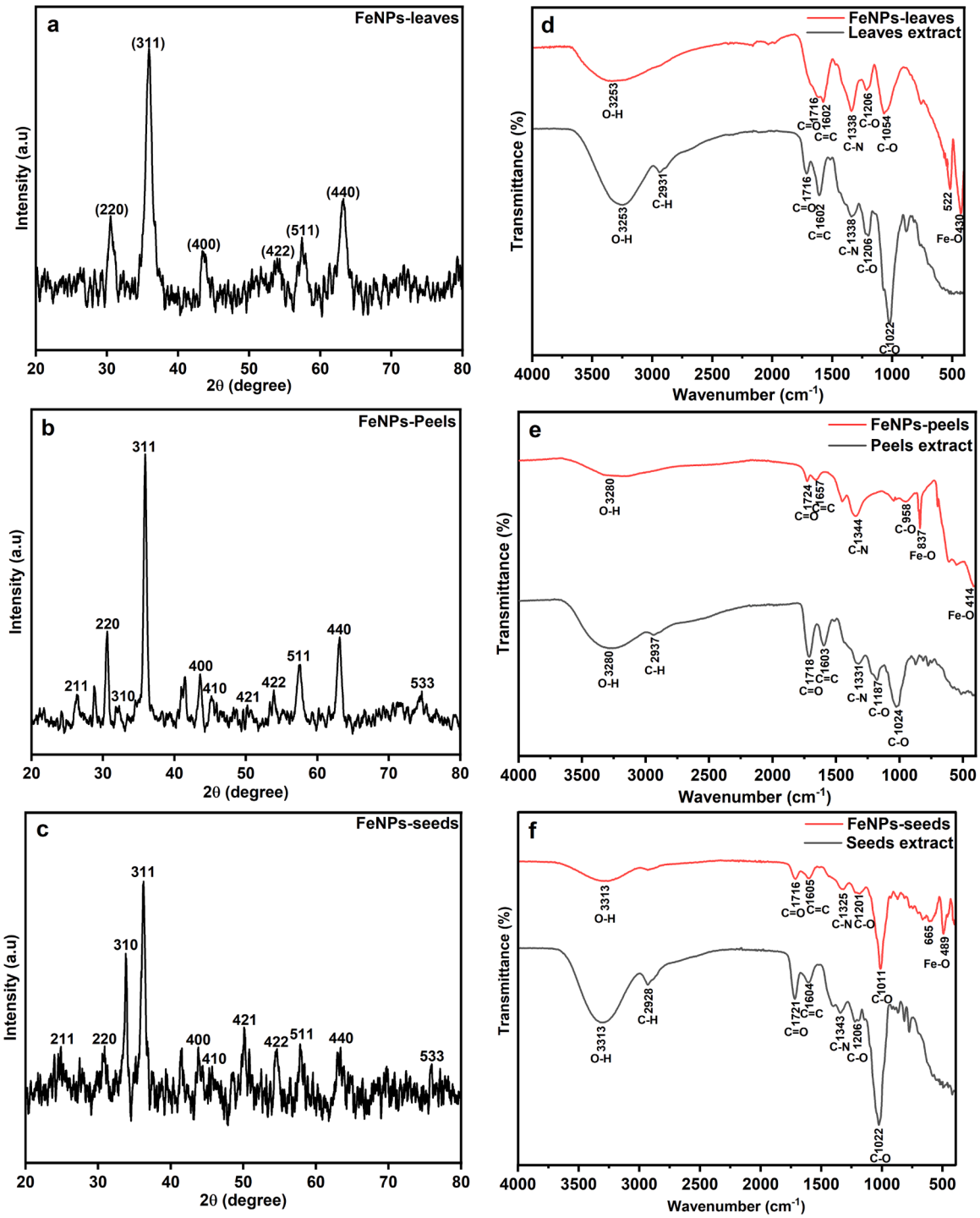

Fig. 5. (a,b,c) XRD patterns of the FeNPs, and (d,e,f) FTIR spectra of the FeNPs and the Punica granatum extracts.

Batch adsorption experiments

Batch adsorption experiments were performed to assess the adsorptive behaviour of the various biogenic synthesized iron oxide NPs towards BTEX removal. Lab-prepared BTEX wastewater was used in the study due to the complicated protocols encountered in obtaining real industrial BTEX wastewater. The effects of parameters, that is, pH (2–12), NPs dosage (0.2–1.0 g/L), contact time (2–80 min), and concentration (20–180 mg/L) on the BTEX adsorption tendency of the iron oxide NPs were investigated.

The adsorption experiments were performed by placing 50 mL of the prepared BTEX solutions in glass bottles, then adding the required dose of the FeNPs to the BTEX solutions, and shaking the suspension at 150 rpm for the specified period of time. The required parameters, which include the pH, NPs dosage, contact time, and BTEX concentration employed in the various adsorption experiments, are stated in the result section. Upon completion of each specific test, the NPs were separated from the BTEX solutions through centrifugation. An aliquot of the BTEX solutions was collected, and then the final concentrations were measured with an Agilent 7890A gas chromatograph instrument (column: 30 m × 0.25 mm ID BP5MS × 0.25 μm), having a flame ionization detector, and paired with an Agilent 7693A series automatic liquid sampler. The flow rate of the nitrogen carrier gas was kept at 2.64mL/min, with an injection volume of 0.2μL in a splitless mode. An oven initial temperature was set and maintained at 40 °C for 2 min, then ramped to 90 °C and held for 3 min at 10 °C/min, then finally to 200 °C and held for 2 min at 20 °C/min.

The adsorption tendency of the NPs was then determined by calculating their adsorption capacity and BTEX removal percentage according to Eqs. (2) and (3), respectively.

$$q_t = \frac{(C_o - C_t)V}{m} \tag{2}$$

$$Removal\ (\%) = \frac{C_o - C_t}{C_o} 100 \tag{3}$$

Where q_t (mg/g) denotes the adsorption capacity, V (L) denotes the volume of the BTEX solution, while m (g) denotes the weight of the NPs adsorbents. C_o (mg/L) and C_t (mg/L) represent, respectively, the initial and final BTEX concentrations.

Results and discussion

Characterization of the Punica granatum extracts

The phenolic compounds are important phytochemicals in the Punica granatum extracts, responsible for reducing the $FeCl_3$ precursor to iron oxide NPs [21]. Their concentration in the Punica granatum extracts can affect the reaction kinetics and the features of the produced nanoparticles [21]. The total phenolic content of the aqueous Punica granatum extracts, reported as the gallic acid equivalents (GAE) per g of dry weight of the Punica granatum parts, showed that the leaves and peels extracts have similar amounts of phenolic content. The leaves extract has a total phenolic content of 47.44 ± 0.58 mg GAE/g dry wt of leaves, and that of the peels extract was 47.16 ± 0.72 mg GAE/g dry wt of peels. A total phenolic content of 0.60 ± 0.02 mg GAE/g of dry wt of seeds was obtained for the seeds extract, thus indicating that the seeds extract has the lowest phenolic content among the three Punica granatum parts. The low total phenolic content of the seeds extract could be responsible for the slower reaction observed during the synthesis of the FeNPs-seeds. As described in section 2.3, the bio-reduction of the iron precursor by the seeds extract took 8 h, while the bio-reduction using the leaves and peels extract was completed in 3 h. Therefore, it can be affirmed that the total phenolic content in the plant extracts may have a direct correlation with the reaction speed during the biogenic synthesis of FeNPs.

The phytochemicals in the Punica granatum extracts were further assessed with GC–MS, and the chromatograms are displayed in Fig. 4. Some of the phytochemicals found in the extracts are depicted in the chromatograms and in Table S1, S2, and S3. Active phytochemicals, such as furfural, 2-isopropoxyphenol, 5-hydroxymethylfurfural, rhamnose, salicylic acid, maltol, and dodecanoic acid were found in the extracts. Thus, in addition to the phenolic compounds, other phytochemicals are present in the plant extracts. As shown in Tables S1, S2, and S3, each extract has distinct varieties of phytochemical compounds, which could exhibit different roles in the bio-reduction of the iron precursor. This suggests that the mechanism of the biosynthesis of the FeNPs using these three extracts may differ, ultimately resulting in nanomaterials with distinct properties and performance.

Characterization of the various iron oxide NPs

Powder X-ray diffraction (PXRD) results

The phase identification of the iron oxide NPs (FeNPs) obtained using powder X-ray Diffraction (PXRD) is shown in Fig. 5 (a–c). In the XRD pattern of the FeNPs-leaves, diffraction peaks were observed at 30.29°, 35.68°, 43.36°, 53.81°, 57.36°, and 62.99°, which are respectively indexed to (200), (311), (400), (422), (511), and (440) planes cubic phase of magnetite (Fe_3O_4) (ICSD collection code 29,129). The FeNPs- peels and FeNPs-seeds displayed similar diffraction peaks at 26.16°, 30.30°, 33.97°, 35.69°, 43.38°, 44.78°, 50.10°, 53.83°, 57.38°, 63.02°, and 74.59° which respectively corresponds to miller indices of (211), (220), (310), (311), (400), (410), (421), (422), (511), (440), and (533) planes of cubic phase of maghemite (Fe_2O_3) (ICSD collection code 250,541). While the peels and seeds extract of the Punica granatum both produced maghemite, the colour of the maghemite differs. Maghemite exists in various colours, including brown, bluish-black, yellow, and yellowish-brown [22]. The FeNPs-peels are bluish-black maghemite, while the FeNPs-seeds are yellowish-brown maghemite, as depicted in Fig. 1. Therefore, the XRD results indicate that different forms of iron oxide were obtained by using the various extracts of Punica granatum to reduce $FeCl_3$. This portrays the complex role of plant phytochemicals in the type of biogenic synthesized NPs obtained using a particular plant extract. As shown in the TPC and GC–MS results of the extracts, the Punica granatum leaves, peels, and seeds have different concentrations of phenolics and varying compositions of phytochemicals. These variations in the concentration and composition of the phytochemicals in the three Punica granatum parts could result in different routes to the bio-reducing process, hence the various types of FeNPs obtained.

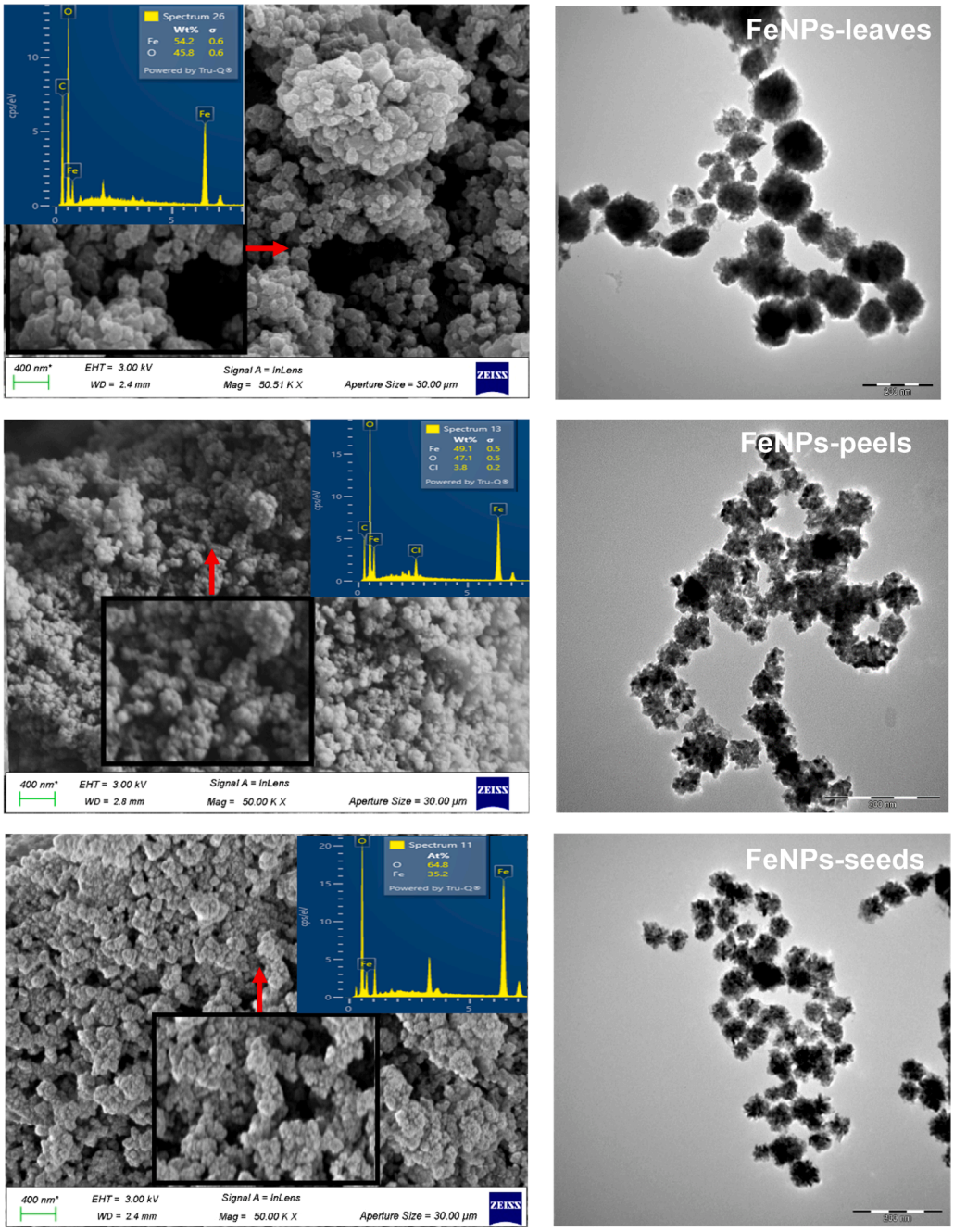

Fig. 6. SEM and TEM image of the FeNPs.

Chemical composition analysis

FTIR was performed to compare the functional groups in the Punica granatum extracts and the subsequent FeNPs and to confirm the capping tendency of the extracts on the FeNPs. The FTIR spectra of the Punica granatum extracts and their subsequent FeNPs in the region 400 – 4000 cm^{-1} are presented in Fig. 5(d–f) and indicate that the leaves extract has a broad band around 3253 cm-1, emanating from the O—H stretching vibration of the phenols and alcohols in the extracts [23,24]. The band at 1716 cm^{-1} could result from the C=O stretching vibration of the carboxylic acid-containing compounds in the extract [23,25]. Bands at 1206 and 1022 cm^{-1} could be due to the C—O stretching vibration of the phenols and alcohols, respectively [23,26]. The other bands at 2931, 1602, and 1338 cm^{-1} could emanate from the asymmetric and symmetric stretching vibrations of the C—H, stretching vibration of C=C, and the stretching vibration of C—N, respectively [23,27,28]. Comparing the spectra of the leaves extract and the FeNPs-leaves, the FeNPs-leaves exhibit bands at 3253, 1716, 1602, 1338, 1206, and 1054 cm^{-1}, which are all similar to the bands observed in the spectrum of the leaves

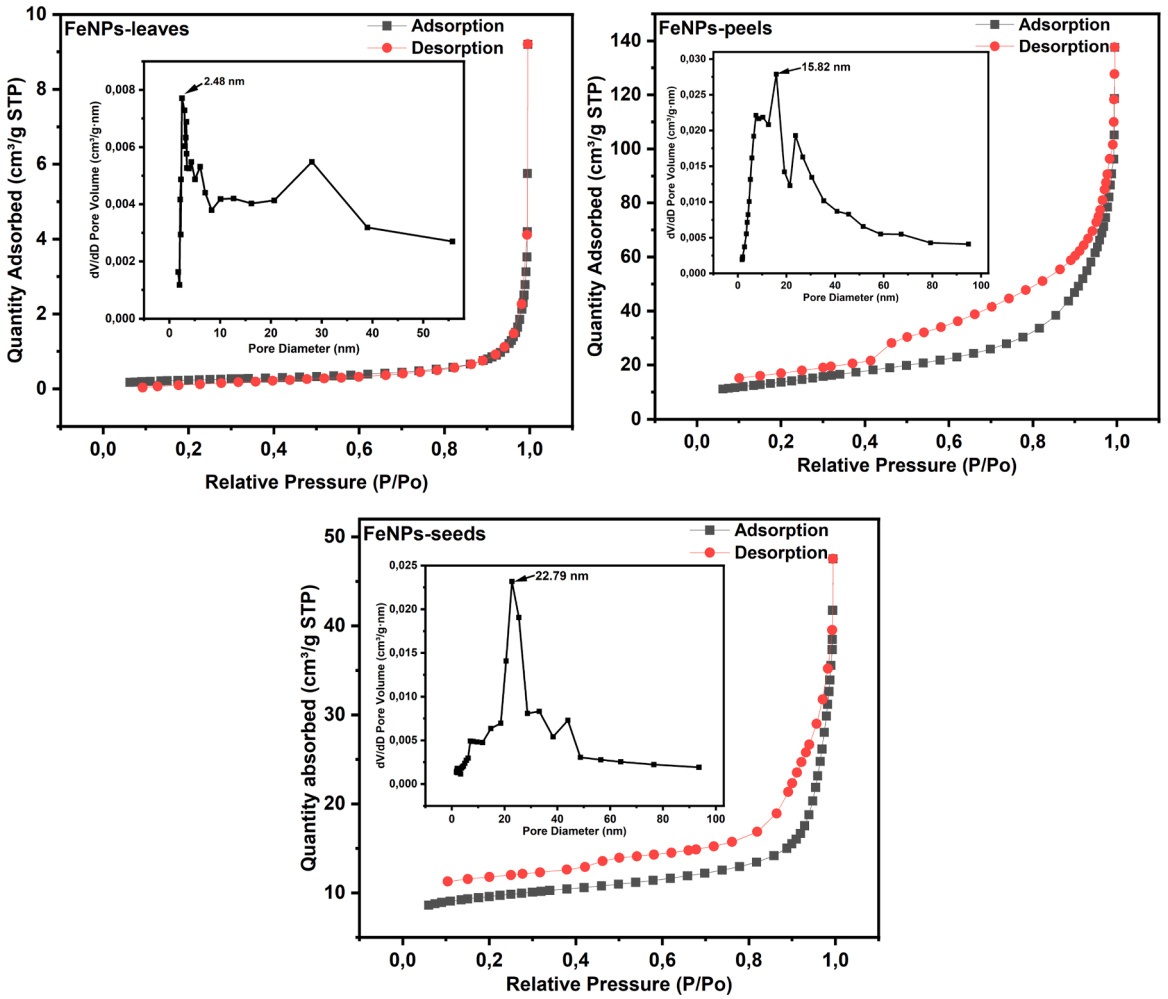

Fig. 7. The N_2 adsorption-desorption isotherms and pore size distributions (inset) of the FeNPs.

extract. This confirms the deposition of some active phytochemicals from the leaves extract onto the surface of the biogenic synthesized FeNPs, thereby capping and stabilizing the FeNPs. The presence of functional groups, including O—H and C—N, on the FeNPs-leaves can also provide more active sites to improve the removal of organic contaminants, such as BTEX, from contaminated wastewater [29]. Additional bands at 522 and 430 cm^{-1} in the FeNPs-leaves spectra correlate with the stretching of Fe-O of the Fe_3O_4.

The spectra of the peels extract show bands at 3280, 2937, 1718, 1603, 1331, and 1024 cm^{-1}, respectively, conforming to the O—H, C—H, C=O, C=C, C—N, and C—O functional groups in the phytochemicals of the extract as previously discussed. Similar bands were observed in the spectra of the FeNPs-peels at 3280, 1724, 1657, 1344, and 958 cm^{-1}, which also conform to O—H, C—H, C=O, C=C, C—N, and C—O functional groups respectively. The seeds extract exhibit bands at 3313, 2928, 1721, 1604, 1343, and 1022 cm^{-1} which are linked to O—H, C—H, C=O, C=C, C—N, and C—O respectively, and the FeNPs-seeds shows bands at 3313, 1716, 1605, 1325, 1201, and 1011 cm^{-1} also corresponding to O—H, C—H, C=O, C=C, C—N, and C—O respectively. This indicates that there is deposition of some active phytochemicals from the peels or seeds extract onto their respective FeNPs, which can cap and stabilize the FeNPs. Some of the identified functional groups, like the O—H and the C—N on the FeNPs, could provide active sites for the removal of organic contaminants, including BTEX [29]. The spectra of the FeNPs-peels show additional bands at 837 and 414 cm^{-1}, while additional bands were seen for the FeNPs-seeds at 665 and 489 cm^{-1}, which are due to the Fe—O of the Fe_2O_3 phase [30]. Therefore, there are phytochemicals on the surface of all three biogenic synthesized FeNPs, which could stabilize the FeNPs, minimize their agglomeration, and provide active sites for BTEX adsorption.

Morphological characterization

SEM and TEM were used to assess the morphology of the FeNPs, and the images are shown in Fig. 6. The SEM images indicate that all the FeNPs are mostly spherical in shape, with fairly good dispersion, as observed in their respective TEM images. The fairly good dispersity of the FeNPs, without any chemical coating on their surface, is due to the natural coating of the FeNPs surfaces by the phytochemicals in the various plant extracts. The FeNPs-leaves seemingly exhibit a more spherically defined structure and have better

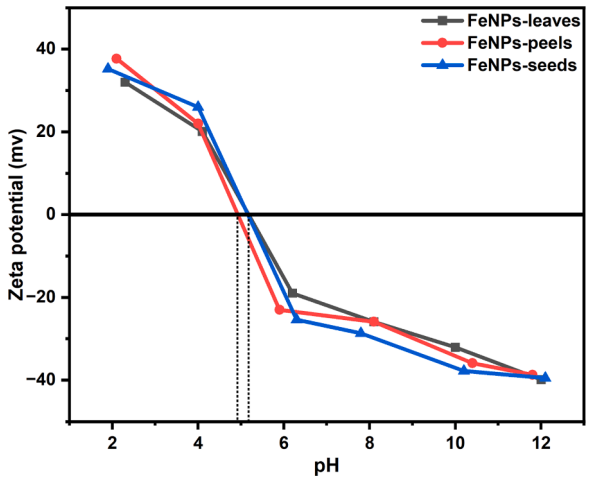

Fig. 8. Zeta potential of the FeNPs.

dispersity than the FeNPs-peels and FeNPs-seeds. Although it is well known that the capping and stabilizing effects of the phytochemicals are responsible for the good dispersity, the correlation between the type and concentration of the phytochemicals and the FeNPs morphology could not be ascertained due to the complexity of the phytochemicals in the plant extracts. All the FeNPs have rough surfaces, as shown in their TEM images. The average particle sizes of the FeNPs were measured and summarized from their TEM images using ImageJ software. FeNPs-leaves have an average particle size of 73.35 ± 8.7 nm, while FeNPs-peels and FeNPs-seeds have average particle sizes of 39.51 ± 6.6 nm and 37.20 ± 7.6 nm, respectively. The reaction times of FeNPs-leaves and FeNPs-peels were shorter than the FeNPs-seeds; hence, it was expected that the particle sizes of FeNPs-leaves and FeNPs-peels would be smaller than the FeNPs-seeds since shorter reaction times typically result in smaller sized nanoparticles [10,31]. The smaller particle size of the FeNPs-seeds, despite its longer synthesis time, further established the complexity of the factors determining the features of biogenic synthesized NPs. In a study investigating the basis and mechanism of phytochemicals in *H. perforatum* plant-based synthesis of Ag NPs conducted by Pradeep et al. [12], it was observed that two phytochemicals, xanthones and phloroglucinols, serve as capping agents in the biogenic synthesis. This shows the uniqueness of the role and mechanism of phytochemicals in the biogenic synthesis of NPs. Therefore, a plausible explanation for the smaller size of the FeNPs-seeds is that the seed extract may contain unique phytochemicals capable of rapidly capping the FeNPs as they form, thereby inhibiting their growth during the longer synthesis process [32]. The FeNPs-leaves and FeNPs-peels also have different particle sizes despite being synthesized over the same duration. All three plant extracts contain a varying composition of phytochemicals, which can have unique roles in the synthesis mechanism and the growth of the FeNPs.

Textural features of the FeNPs

BET analysis was performed to determine the textural features of the FeNPs in terms of their porous nature and specific surface area, and the nitrogen adsorption/desorption isotherm curves obtained using the BET technique are presented in Fig. 6. As established from the IUPAC classification of the isotherm curves, all the FeNPs had type IV isotherms, which indicates their mesoporous nature. Mesoporous materials are notably suitable adsorbents for removing many organic contaminants from wastewater [33]. Hence, the FeNPs could be potential adsorbents for target organic contaminants, such as BTEX. Among all the FeNPs, FeNPs-peels have the highest BET specific surface area of 48.45 m^2/g, while the FeNPs-seeds have a specific surface area of 35.40 m^2/g. The FeNPs-leaves have the lowest specific surface area at 8.61 m^2/g. Here again, the uniqueness of the various phytochemicals in the plant extracts may have resulted in the varying features of the three biogenic synthesized FeNPs.

The FeNPs pore sizes were assessed using the Barrett-Joyner-Halenda (BJH) method from the desorption branch. The insets of Fig. 7 show the respective pore sizes of the FeNPs, which further establishes mesopores in the FeNPs. Mesoporous materials typically have pore diameters between 2 - 50 nm [34], and most of the pores of the FeNPs are within this range, as shown in the insets of Fig. 7. The pore sizes with the highest pore volumes are 2.48 nm, 15.82 nm, and 22.79 nm for FeNPs-leaves, FeNPs-peels, and FeNPs-seeds, respectively. The BET results of the FeNPs indicate their effective porous nature and potential application as adsorbents for organic contaminants such as BTEX.

Zeta potential results

The zeta potential measurements were conducted to determine the surface charge of the FeNPs at the measured pH range between 2 and 12, as shown in Fig. 8. At lower pHs, all three FeNPs have high zeta potential and are positively charged. This behaviour of the FeNPs at lower pHs could be due to the protonation of their surface groups at the lower pH ranges. As shown in their FTIR, the FeNPs surface has functional groups, which include the hydroxyl and amine groups, that tend to be protonated at low pH. Moreover, metal oxides have the tendency to hydrate in an aqueous solution, thereby having its surfaces covered with hydroxyl groups, which could be protonated at low pH [35,36]. The protonation of these surface groups on the FeNPs resulted in positively charged NPs at the low pHs.

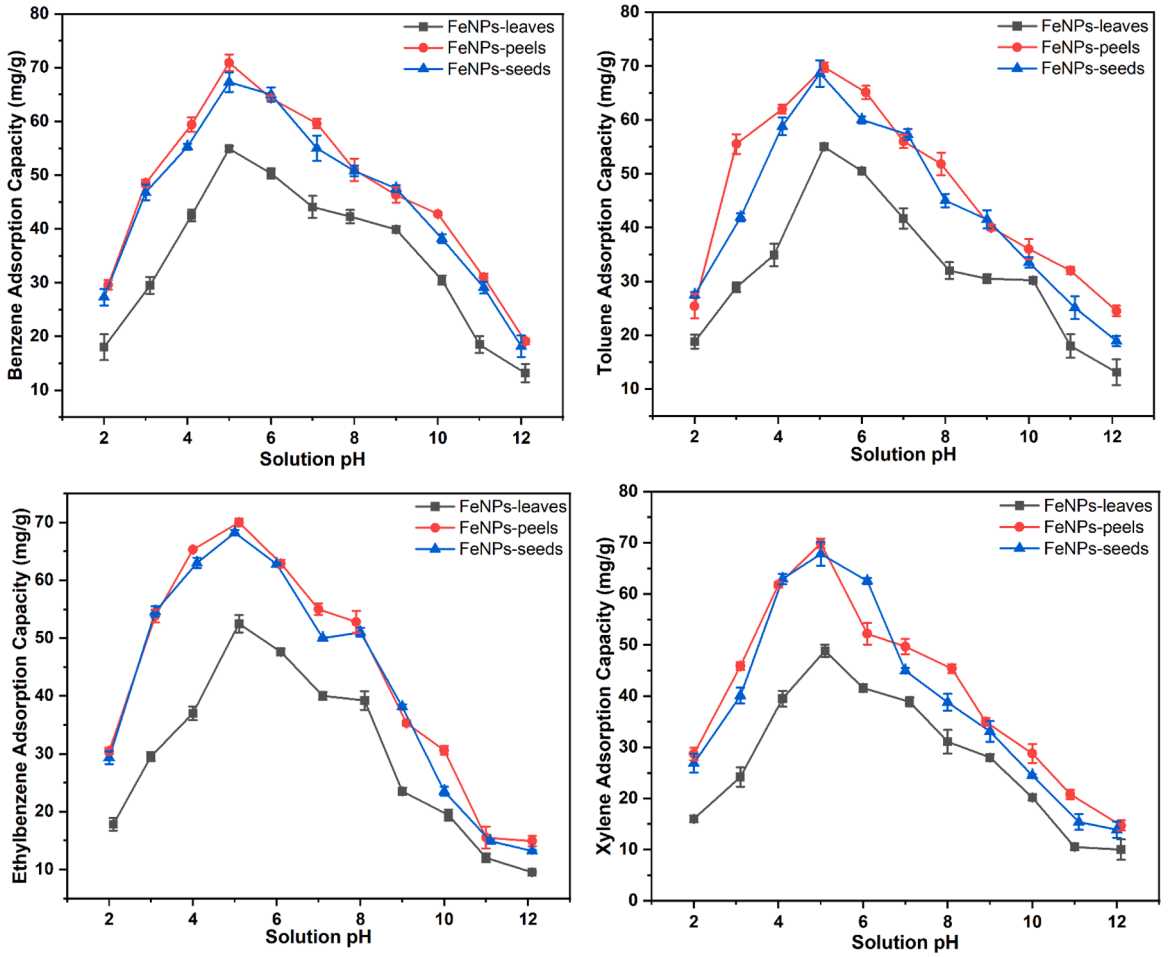

Fig. 9. Effect of solution pH on BTEX adsorption onto the FeNPs.

At a pH of 4.92, the FeNPs-peels established its point of zero charge (pH_{pzc}), while the pH_{pzc} of the FeNPs-leaves and the FeNPs-seeds was 5.18. Above the pH_{pzc}, the surface charge of the FeNPs becomes negative, which can be ascribed to the deprotonation of the aforementioned functional groups on their surfaces at higher pHs [36]. As the pHs were increased, the zeta potentials of all the FeNPs became more negative, reaching -39.9, -38.7, and -39.5 at pH 12 for the FeNPs-leaves, FeNPs-peels, and FeNPs-seeds, respectively. The results of the zeta potential of the FeNPs could provide an understanding of their behaviour towards BTEX adsorption at various pHs.

BTEX adsorption study

Effect of solution pH on BTEX adsorption

The initial pH of the solution is a vital parameter that can affect the behaviour of the FeNPs adsorbents towards the adsorption of the BTEX [37]. According to the zeta potential results in Fig. 8, the FeNPs exhibit varying surface charges at different pHs, and the surface charges of the FeNPs influence the interaction between the FeNPs adsorbents and the BTEX adsorbate [37]. Hence, the impact of the solution pH on BTEX adsorption using the FeNPs was determined at different pHs (2 – 12) for 40 min. 10 mg of FeNPs and 20 mg/L (50 mL) of the BTEX solution were used for the test. As depicted in Fig. 9, the adsorption capacity of the FeNPs towards all the constituents of BTEX (that is, benzene, toluene, ethylbenzene, and xylene) increased as the pH increased and attained its highest at pH 5. This behaviour at lower pH can be elucidated by the ability of iron oxide to accept protons under acidic conditions to form positively charged species [38]. Thus, the positive charge favours electrostatic interaction between the FeNPs and the π-electrons of the BTEX. However, the π-electrons interaction relies on the available active sites on the FeNPs [39]. With the FeNPs interacting with the H^+ at low pH, the available active sites for it to interact with the π-electrons of the BTEX decrease. As the pH increases, there is a reduced amount of H^+, thus reducing the amount of H^+ interacting with the FeNPs, thereby providing more active sites for the π-electrons interaction with the FeNPs. Above pH 5, the adsorption capacity started to decrease. As shown in Fig. 8, the surface charges of the FeNPs were negative above pH 5. In addition, there was the presence of OH^- at higher pHs. The negative surface charge of the FeNPs above pH 5 and the OH^- in the solution repelled the π-electrons of the BTEX, thereby diminishing the interaction between the FeNPs

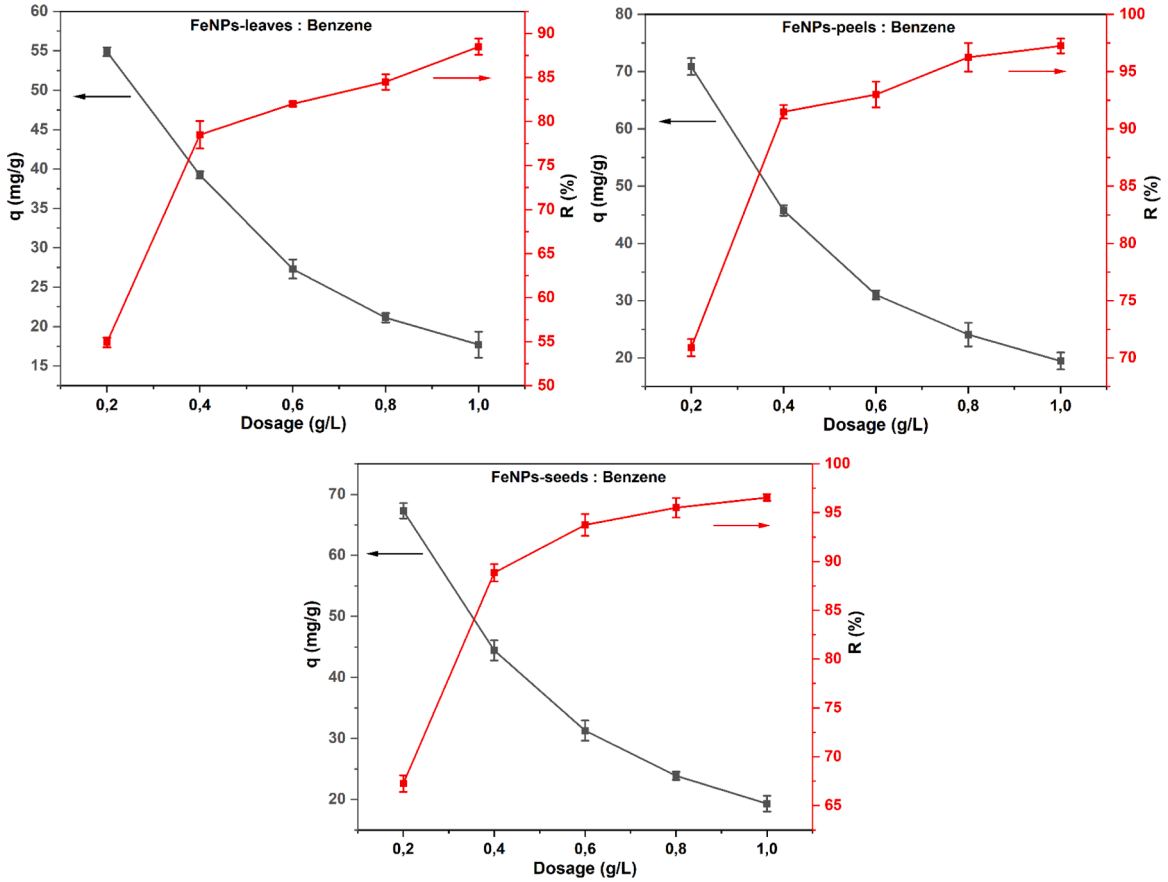

Fig. 10. Effect of FeNPs dosage on benzene adsorption.

Table 1
Effect of FeNPs dosage on toluene, ethylbenzene, and xylene adsorption.

Pollutant	Dosage (g/L)	FeNPs-leaves		FeNPs-peels		FeNPs-seeds	
		q (mg/g)	R (%)	q (mg/g)	R (%)	q (mg/g)	R (%)
Toluene	0.2	55.10±1.74	55.10±1.74	69.80±2.38	69.80±2.38	68.60±1.54	68.60±1.54
	0.4	37.75±1.03	75.50±1.88	45.30±1.54	90.60±1.67	45.90±2.30	91.80±1.50
	0.6	28.17±1.83	84.50±1.02	31.50±0.90	94.50±1.82	30.97±2.75	92.90±2.72
	0.8	21.56±1.68	86.25±0.93	24.09±1.85	96.35±1.77	24.05±1.55	96.20±1.10
	1.0	17.61±0.55	88.05±2.25	19.55±1.87	97.75±0.95	19.45±0.99	97.25±2.83
Ethylbenzene	0.2	52.50±2.50	52.50±2.50	70.45±2.71	70.45±2.71	68.20±0.93	68.20±0.93
	0.4	37.96±1.94	75.90±1.40	43.59±1.71	87.85±1.97	44.50±1.75	89.00±1.64
	0.6	25.82±2.24	77.45±1.95	31.63±2.59	94.90±1.58	31.04±2.10	93.10±0.75
	0.8	20.50±1.25	82.00±0.80	24.05±1.67	96.20±1.08	23.95±0.75	95.80±2.50
	1.0	17.52±1.83	87.60±1.44	19.63±0.95	98.15±1.85	19.24±0.50	96.20±0.80
Xylene	0.2	48.95±1.14	48.95±1.14	69.90±0.46	69.90±0.46	67.85±0.91	67.85±0.91
	0.4	35.65±2.04	71.30±1.53	43.82±1.27	87.65±1.25	44.25±1.28	88.50±1.00
	0.6	25.80±1.28	77.40±1.06	30.97±0.77	92.90±0.80	30.02±0.32	90.05±0.82
	0.8	21.93±0.85	87.70±0.91	24.18±1.19	96.70±0.91	23.50±0.25	94.00±1.50
	1.0	17.64±0.82	88.20±0.25	19.48±0.78	97.40±1.10	19.02±0.64	95.10±1.12

and the BTEX; hence, the decrease in adsorption capacity obtained at higher pHs.

The FeNPs-leaves exhibited the lowest BTEX adsorption across all the tested pHs, while the FeNPs-peels and FeNPs-seeds showed fairly the same BTEX adsorption performance. The lower BTEX adsorption of the FeNPs-leaves could be due to its lower specific surface area, as previously reported in its BET results.

Since it has been established that the pH has a considerable effect on the adsorption performance of the FeNPs, the subsequent adsorption experiments were maintained at a specific pH, and the optimum pH 5 was chosen.

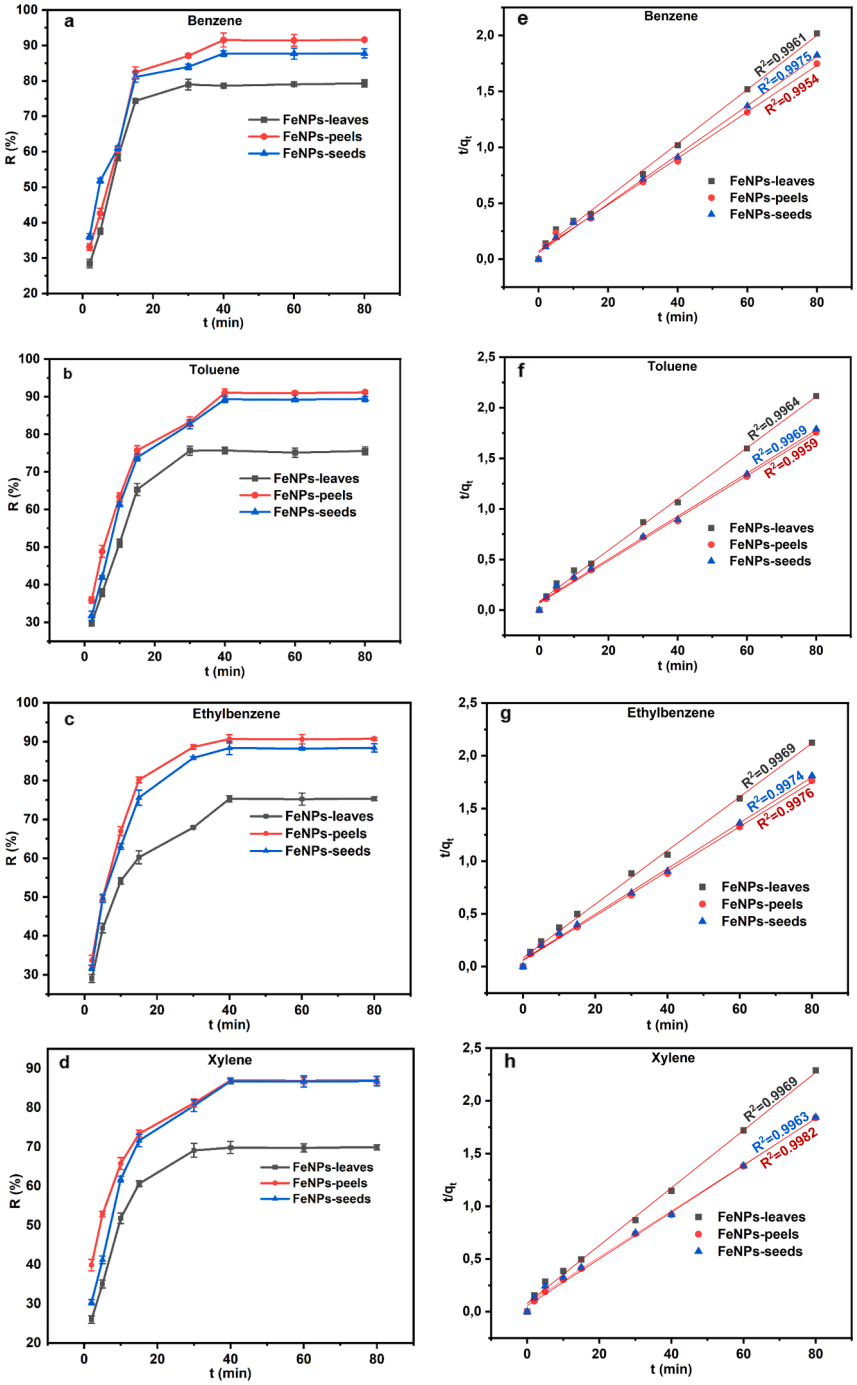

Fig. 11. (a, b, c, d) Effect of contact time on BTEX adsorption on the FeNPs, and (e, f, g, h) their respective linear fit for pseudo-second-order kinetic model.

Effect of FeNPs adsorbent dosage

This test was performed to assess the influence of the FeNPs dosages on the adsorption and removal efficiency of BTEX at pH 5 using 50 mL (20 mg/L) of BTEX solution for a duration of 40 min while varying the NPs dosage from 0.2 g/L to 1.0 g/L. As depicted in Fig. 10 and Table 1, the BTEX adsorption capacity decreased as the FeNPs dosage increased, while their corresponding BTEX percentage removal increased. This decline in the adsorption capacity could be directly linked to the increased number of the FeNPs adsorbent with constant BTEX concentration. On the other hand, the increment in the BTEX percentage removal was a result of the increased availability of the adsorption sites and surfaces as more adsorbents were introduced at constant BTEX concentration, thereby

Table 2
Kinetic pseudo-first and pseudo-second-order parameters of BTEX adsorption by the FeNPs.

Adsorbent	Pollutant	$q_{e,\ exp}$ (mg/g)	PFO		PSO	
			$q_{e,\ cal}$ (mg/g)	k_1 (min^{-1})	$q_{e,\ cal}$ (mg/g)	k_2 (g/mg/min)
FeNPs-leaves	Benzene	39.52	19.11	0.0986	41.49	0.0084
	Toluene	37.80	25.01	0.0873	39.53	0.0075
	Ethylbenzene	37.61	33.83	0.1271	39.37	0.0077
	Xylene	34.95	22.81	0.1191	36.49	0.0094
FeNPs-peels	Benzene	45.75	35.11	0.1183	48.08	0.0060
	Toluene	45.47	35.69	0.1066	47.62	0.0064
	Ethylbenzene	45.31	33.02	0.1329	47.17	0.0078
	Xylene	43.50	32.85	0.1234	45.04	0.0089
FeNPs-seeds	Benzene	43.88	32.99	0.1315	45.45	0.0086
	Toluene	44.70	38.29	0.1135	46,.95	0.0058
	Ethylbenzene	44.20	31.04	0.1234	46.08	0.0074
	Xylene	43.39	32.36	0.1351	45.66	0.0061

increasing the removal efficiency. Thus, this test established that there is a considerable effect on the adsorption performance of the FeNPs as their dosages are varied. Comparing the three FeNPs, the FeNPs-peels and FeNPs-seeds exhibited higher adsorption capacity than the FeNPs-leaves. This could also be due to the higher specific surface area of FeNPs-peels and FeNPs-seeds.

Effect of contact time and adsorption kinetics

The impact of contact time on the BTEX adsorption performance of the FeNPs adsorbents was studied at pH 5 using 20 mg of FeNPs and a 20 mg/L (50 mL) BTEX solution, with the contact time varying from 2 min to 80 min. The result, as depicted in Fig. 11(a–d), shows that all three FeNPs adsorbents exhibited similar adsorption trends when the contact time was varied. From the results, the adsorption of BTEX onto the different NPs initially occurred rapidly until 15 min; then, the adsorption rate gradually slowed until equilibrium was attained at 40 min. This behaviour can be attributed to the high available active sites on the adsorbents at the initial stages of the adsorption, thus accelerating the adsorption of BTEX at the early stages. As the adsorption process proceeded, the available active sites gradually decreased, resulting in a slower adsorption rate until all the sites were saturated at the equilibrium stage.

To understand the adsorption kinetic process, pseudo-first-order (PFO) and pseudo-second-order (PSO) models were employed to fit the obtained adsorption data and calculate the kinetic parameters. The linearized form of the models used to determine the adsorption kinetic parameters are expressed as follows:

Pseudo-first-order model:

$$\log\ (q_e - \ q_t) = \log\ \ q_e - \ \frac{k_1 t}{2.303} \tag{4}$$

Pseudo-second-order model:

$$\frac{t}{q_t} = \ \frac{1}{k_2 q_e{}^2} + \ \frac{t}{q_e} \tag{5}$$

The q_e (mg/g) and q_t (mg/g) in the equations denote, respectively, the adsorption capacity at equilibrium time and time t (min); t (min) is the adsorption time; k_1 (min^{-1}) and k_2 ($gmg^{-1}min^{-1}$) are, respectively, the rate constants of the pseudo-first-order and pseudo-second-order models.

Fig. S3 depicts the fitting curves for the pseudo-first-order, while those for the pseudo-second-order are depicted in Fig. 10(e–h). Their relative kinetic parameters are presented in Table 2. As shown in the fitting curves, it is evident that the pseudo-second-order model correlates more accurately with the adsorption process than the pseudo-first-order, as inferred from the higher correlation coefficient (R^2) of the pseudo-second-order model. Additionally, the q_e values ($q_{e,\ cal}$) calculated from the pseudo-second-order were more accurately closer to the experimentally determined values ($q_{e,\ exp}$), as depicted in Table 2. For instance, the calculated q_e values ($q_{e,\ cal}$) for FeNPs-leaves adsorption of benzene were 19.11 mg/g and 41.49 mg/g for the pseudo-first-order and the pseudo-second-order models, respectively, while the experimentally obtained value was 39.52 mg/g. Thus, indicating that the pseudo-second-order model gave a more accurate representation of the BTEX adsorption process on the FeNP adsorbents. Pseudo-second-order model typically represents chemisorption processes [40]; hence chemisorption was established to be the rate-controlling step in the BTEX adsorption process using the biogenic-synthesized FeNPs.

Effect of initial concentration and adsorption isotherms

The adsorption performance of the FeNPs adsorbents was assessed at different initial concentrations ranging from 20 mg/L to 180 mg/L of the BTEX solution (50 mL) at pH 5 using 20 mg of the FeNPs for a duration of 40 min. The results, as presented in Fig. 12, show that the percentage removal, R (%), of BTEX using the FeNPs decreased as the concentrations increased. This could be due to the decline in the number of available sites on the FeNPs adsorbents as the BTEX concentration increased, thereby reducing the removal efficiency of the FeNPs adsorbents towards BTEX. Thus, the use of the biogenic-synthesized FeNPs in the adsorptive removal of BTEX is

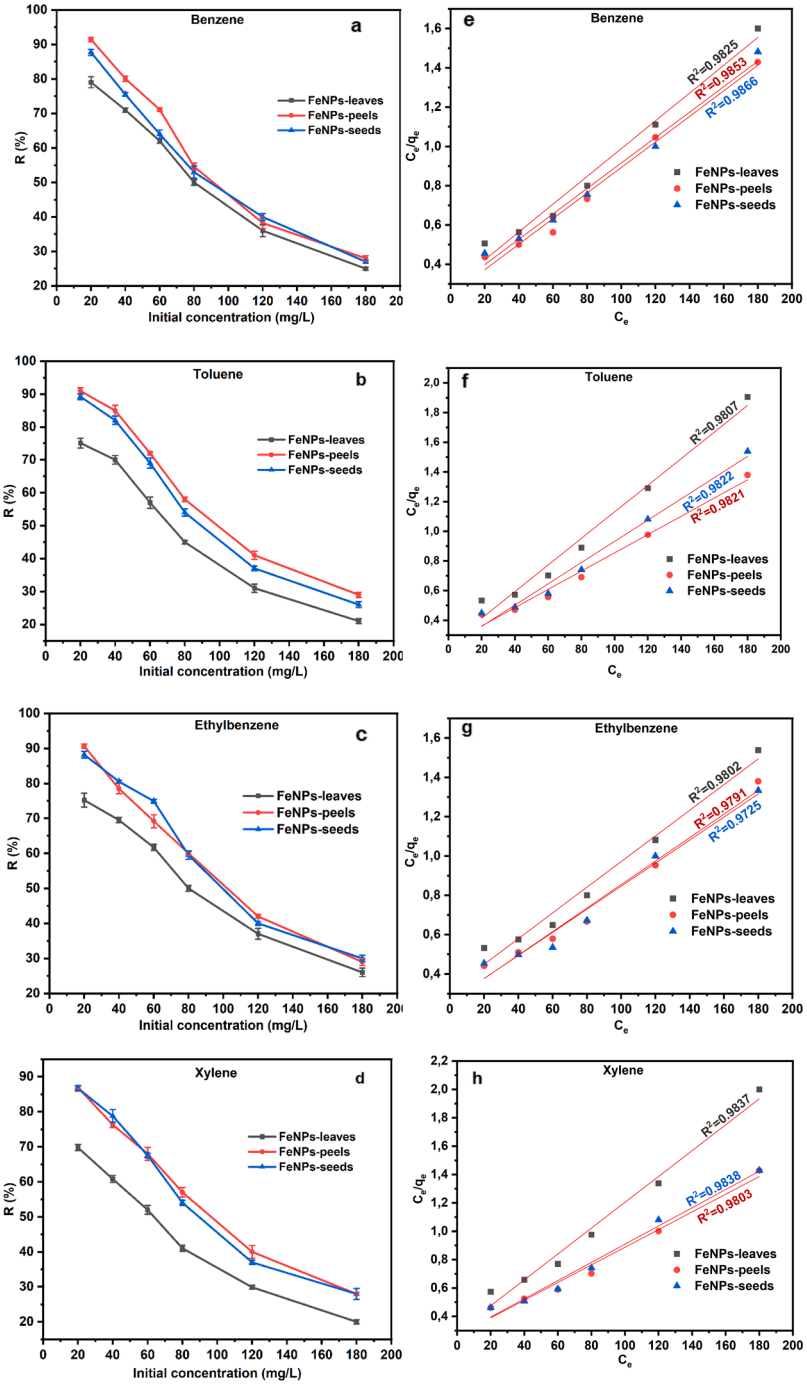

Fig. 12. (a, b, c, d) Effect of BTEX initial concentration on their adsorption on the FeNPs, and (e, f, g, h) their subsequent linear fit for Langmuir isotherm model.

more effective at low BTEX concentrations.

To gain insights into the nature of the adsorption process, the experimental adsorption data was fitted with two isotherm models: Langmuir and Freundlich models. Langmuir model describes monolayer adsorption processes and homogenous interactions at the surface of the adsorbent, with every site on the adsorbent having equal and uniform affinity towards the adsorbate [41]. On the other hand, the Freundlich model mainly describes multilayer adsorption processes on heterogeneous surfaces of the adsorbents, and the affinity of the active sites of the adsorbent towards the adsorbate does not need to be uniform [41]. The fitting of the experimental adsorption data using these models was performed using the linear form of the models according to the below expressions:

Table 3
Langmuir and Freundlich isotherm parameters of BTEX adsorption by the FeNPs.

Adsorbent	Pollutant	Langmuir		Freundlich	
		q_m (mg/g)	K_L (L/mg)	K_F (mg/g)	n
FeNPs-leaves	Benzene	140.85	0.025	11.51	2.44
	Toluene	111.11	0.038	13.86	2.63
	Ethylbenzene	153.85	0.020	9,.69	2.01
	Xylene	109.89	0.031	11.48	2.33
FeNPs-peels	Benzene	153.60	0.027	14.34	2.25
	Toluene	161.29	0.026	13.67	2.15
	Ethylbenzene	166.67	0.023	12.32	2.05
	Xylene	161.29	0.024	12.00	2.06
FeNPs-seeds	Benzene	154.56	0.027	12.49	2.14
	Toluene	138.89	0.033	15.51	2.38
	Ethylbenzene	169.49	0.023	12.18	2.03
	Xylene	156.25	0.024	12.96	2.16

Table 4
A comparison of the adsorption capacities of various iron/iron oxide nanoparticles adsorbents in BTEX adsorption.

Adsorbent and their synthetic route	Adsorbent dosage (g/L)	Temp. (°C)	q_m (mg/g)				Reference
			B	T	E	X	
Nano zero-valent iron (chemical method)	0.22	40	6.3	66,.75	81.44	53.62	[42]
Iron oxide nanoparticles (chemical method)	1.00	25	0.09[a]				[43]
Iron oxide nanoparticles[b] (biosynthetic method)	0.4	25	153.60	161.29	166.67	161.29	This study

[a] Reported as cumulative q_m value [43].
[b] q_m value for FeNPs-peels (This study).

Langmuir isotherm model:

$$\frac{C_e}{q_e} = \frac{1}{K_L q_m} + \frac{C_e}{q_m} \tag{6}$$

Freundlich isotherm model:

$$In\ q_e = In\ K_F + \frac{1}{n}\ In\ C_e \tag{7}$$

with q_e (mg/g) and q_m (mg/g) denoting, respectively, the equilibrium adsorption capacity and the maximum adsorption capacity. C_e (mg/L) denotes the equilibrium concentration of the BTEX solution, K_L (L/mg) denotes the Langmuir constant, K_F (mg/g) is the Freundlich constant, and n corresponds to the adsorption density relating to the feasibility of the adsorption process. Because of the high volatility of BTEX, the adsorption isotherm study was performed only at room temperature.

The plots of $\frac{C_e}{q_e}$ vs C_e (for Langmuir isotherm) and $In\ q_e$ vs $In\ C_e$ (for Freundlich isotherm) are, respectively, presented in Fig. 12 and Fig. S4. The subsequent isotherm parameters, as presented in Table 3, were calculated from the related isotherm plot, that is; q_m and K_L were calculated from the $\frac{C_e}{q_e}$ vs C_e Langmuir isotherm plot while K_F and n were calculated from the $In\ q_e$ vs $In\ C_e$ Freundlich isotherm plot.

The R^2 obtained from fitting the adsorption data with the Langmuir isotherm model was higher than the R^2 obtained from the Freundlich isotherm model, as shown in their respective plots. This suggests that the BTEX adsorption onto the FeNPs adsorbents occurred through monolayer adsorption with homogenous interaction of the BTEX at the FeNPs surfaces.

The comparison of the performance of the FeNPs and other adsorbents is shown in Table 4, and indicates that the calculated maximum adsorption capacity (q_m) established in this study was relatively high compared to other similar studies that utilized iron oxide nanoparticles as a single adsorbent for BTEX removal. Note that the parameters, such as the adsorbent dosage, temperature, and BTEX solution concentrations, used in the different adsorption studies differ; hence, the comparison may not directly relate and compare the performance of the iron oxide used in the various studies.

Possible adsorption mechanism

A series of interactions may be responsible for the adsorptive removal of BTEX using biogenic-synthesized iron oxide NPs, which depends on the properties of the iron oxide NPs and the BTEX. Based on the NPs characterization and adsorption results, three possible mechanisms are depicted in Fig. 13. Mechanism A, as shown in Fig. 13, involves electrostatic interaction between the charged iron oxide nanoparticles and the π electrons of the BTEX. Metal oxide NPs hydrate in an aqueous solution, resulting in an M-OH hydrated form [36]. Under acidic or basic conditions, the M-OH can either be protonated or deprotonated, leading to the formation of $M\text{-}OH_2^+$

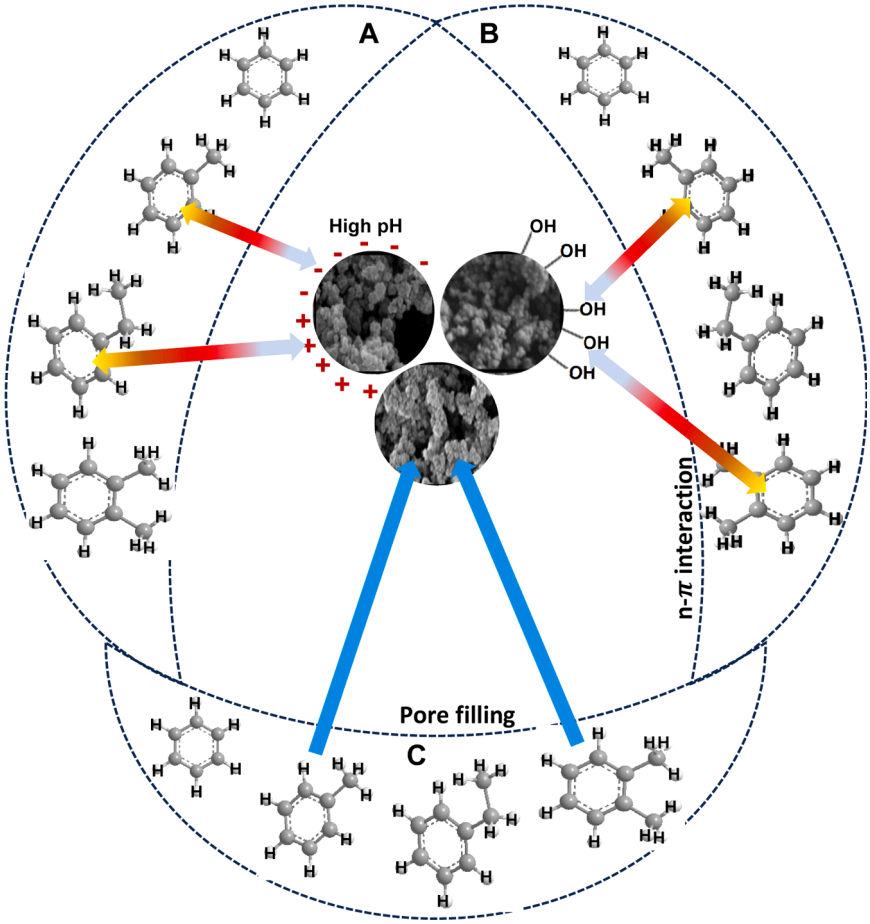

Fig. 13. Schematic diagram of the possible adsorption mechanism of BTEX on the FeNPs.

(acidic) or M-O^{-} (basic). At low pH, there is electrostatic attraction between positively charged NPs and the π electrons of the BTEX [44]; thus necessitating the adsorption of the BTEX to the NPs. In mechanism B, the presence of functional groups, including carboxylic acid and hydroxyl groups on the surface of the iron oxide nanoparticles, as shown in their FTIR results, initiate an OH- π interaction between the NPs and the BTEX. Such OH- π interaction is often responsible for the adsorption of aromatic compounds, such as BTEX on hydroxylated NPs [45,46]. Adsorption could also occur according to mechanism C, that is, through pore filling by diffusion. This is inferred from BET analysis of the NPs, which revealed that the NPs are mesoporous materials with porous structures ideal for adsorbing organic contaminants such as BTEX. Hence, BTEX could be absorbed into the NPs' pore cavities through pore filling.

Regeneration of the biogenic-synthesized FeNPs

The regeneration study was performed to assess the plausibility of reusing the biogenic-synthesized FeNPs after their application for BTEX adsorption. This was achieved through adsorption-desorption experiments, where methanol was used to desorb the BTEX after each adsorption application. The used FeNPs were put in methanol and stirred for 1 h, and then filtered and re-applied for further BTEX adsorption. The process was replicated four times, and the %R was measured after each cycle. Fig. 14 depicts the results of the regeneration study, which demonstrate a decline in the BTEX removal efficiency of the FeNPs after the first adsorption-desorption experiment. The decline could be due to the washing off of some of the active functional groups on the FeNPs during the initial desorption process, thereby reducing the active sites on the FeNPs. However, there were slight changes in the %R of the FeNPs after the subsequent adsorption-desorption cycles. This suggests that some stable, active functional groups on the FeNPs surface may remain after the initial desorption. Combined with the diffusion of BTEX into the pores of the FeNPs, high removal of BTEX was still achieved after each cycle; thus, the FeNPs can be reused for multiple BTEX adsorption. This established the biogenic-synthesized FeNPs as a potential adsorbent for multiple uses in the removal of BTEX from contaminated wastewater.

Limitations of the study

While Punica granatum plant extracts produce FeNPs ideal for removing BTEX from wastewater, some limitations need to be

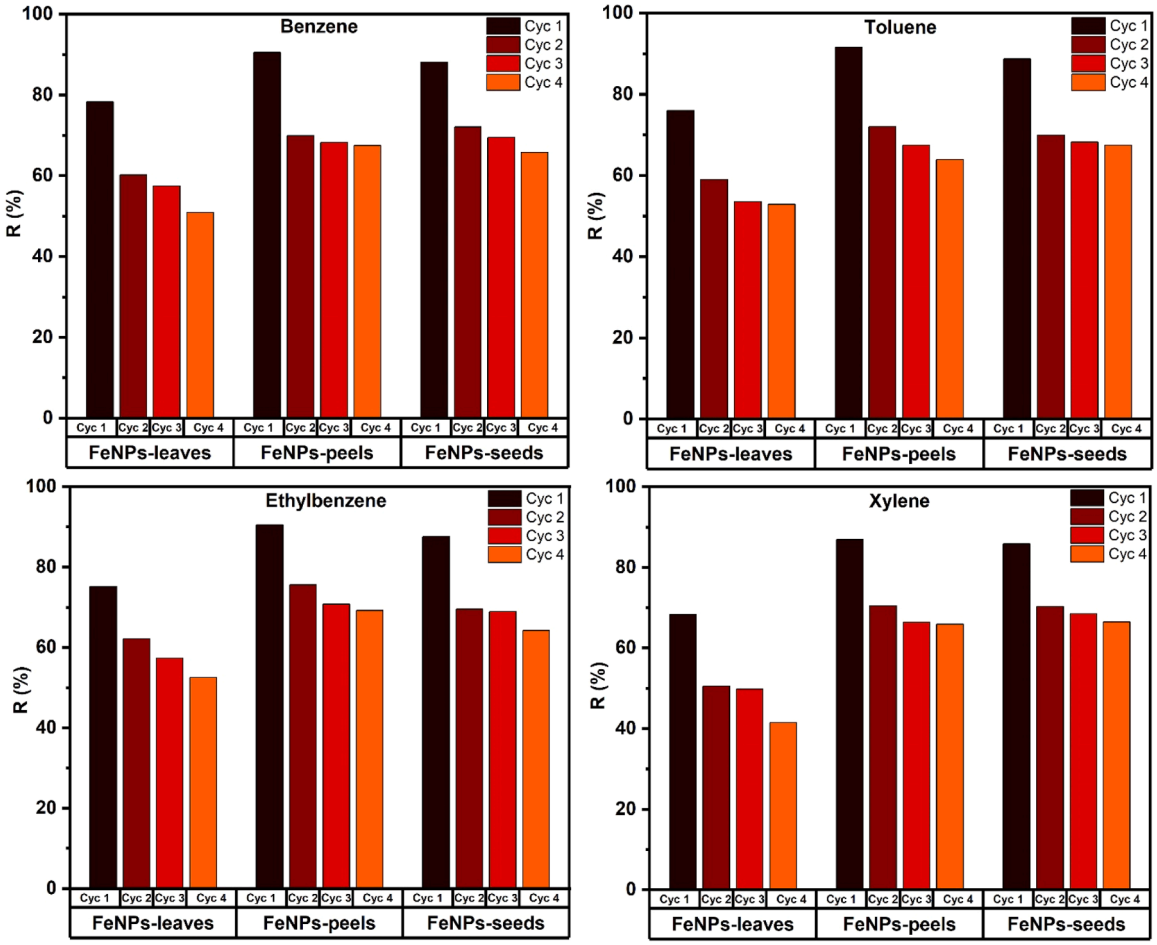

Fig. 14. Regeneration of the various FeNPs in BTEX adsorption.

considered for their large-scale synthesis and applications. First, the concentration of phytochemicals in the various plant extracts (leaves, peels, and seeds) may vary depending on the plant species, maturity, and season. This will impact the FeNPs yield, subsequently influencing their performance in BTEX removal. Also, translating batch synthesis into continuous production and application in industrial BTEX wastewater treatment systems was not investigated in this study. Moreover, in real wastewater containing other contaminants, such as salts, inorganic, and other organic contaminants, FeNPs may undergo transformation of the surface active functional groups, which could adversely impact their performance in BTEX removal. The co-contaminants can also foul the FeNPs surface, blocking the active sites on the nanoparticle surface, leading to reduced BTEX uptake. Furthermore, the possible leaching of iron from degraded FeNPs after long-term application of the FeNPs should be investigated and considered, as this could lead to secondary contamination.

Conclusion

This work identified the potential of Punica granatum-mediated FeNPs as an adsorbent for the BTEX removal from contaminated wastewater. Based on the impact of the phytochemical composition of Punica granatum parts on the properties of the resulting FeNPs, an assessment was conducted to determine the Punica granatum part that yields FeNPs with ideal features for optimal BTEX removal. The Punica granatum leaves, peels, and seeds have different amounts of phenolic compounds and different varieties of phytochemicals, as indicated by the TPC measurement and GC–MS results. Subsequently, FeNPs with distinct features were obtained from the bio-reduction using the three Punica granatum parts. FeNPs-peels and FeNPs-seeds exhibited higher BTEX adsorption capacity than the FeNPs-leaves. The BTEX adsorption capacity of FeNPs-peels at a 0.2 g/L BTEX concentration, pH 5, and 40 min of adsorption time is: B, 70.90 mg/g; T, 69.80 mg/g; E, 70.45 mg/g; and X, 69.90 mg/g. Therefore, to achieve optimal BTEX adsorptive removal using Punica granatum-mediated FeNPs, the Punica granatum peels should be utilized for the biosynthesis; however, the seeds extract can also yield FeNPs with good BTEX adsorptive performance. Pseudo-second-order kinetic model and Langmuir isotherm model best describe the adsorption process. This indicates that BTEX adsorption onto the FeNPs occurred through a chemisorption process, with monolayer adsorption and a homogeneous interaction of the BTEX on the FeNPs surfaces. Further studies should be conducted to establish the

underlying role of the specific phytochemicals in each Punica granatum part in the FeNPs biosynthesis and the mechanism resulting in the distinct features of the FeNPs.

CRediT authorship contribution statement

Ngozi Enemuo: Writing – review & editing, Writing – original draft, Visualization, Validation, Software, Resources, Project administration, Methodology, Investigation, Funding acquisition, Formal analysis, Data curation, Conceptualization. **Michael O. Daramola:** Writing – review & editing, Visualization, Validation, Supervision, Software, Project administration, Methodology, Investigation, Formal analysis, Data curation, Conceptualization. **Heidi Richards:** Visualization, Validation, Supervision, Resources, Project administration, Methodology, Investigation, Funding acquisition, Formal analysis, Data curation, Conceptualization.

Declaration of competing interest

The authors declare that they have no known competing financial interests or personal relationships that could have appeared to influence the work reported in this paper.

Supplementary materials

Supplementary material associated with this article can be found, in the online version, at doi:10.1016/j.sciaf.2025.e03136.

References

[1] P.M. Wanjala, B.K. Opoku, E. Ibisime, E.N. Wafula, Assessment of the impact of benzene, toluene, ethylbenzene, and xylene (BTEX) on soil microbial population in selected areas of Port Harcourt City, Nigeria', Sci. Afr. 27 (Mar. 2025) e02525 https://doi.org/10.1016/j.sciaf.2024.e02525.

[2] B. Yu, Z. Yuan, Z. Yu, F. Xue-song, BTEX in the environment: an update on sources, fate, distribution, pretreatment, analysis, and removal techniques, Chem. Eng. J. 435 (May 2022) 134825, https://doi.org/10.1016/j.cej.2022.134825.

[3] N. Enemuo, H. Richards, M.O. Daramola, Evaluation of the performance of Fe3O4-NPs/PVDF nanocomposite membrane for removal of BTEX from contaminated water, J. Water Process Eng. 60 (Apr. 2024) 105185, https://doi.org/10.1016/j.jwpe.2024.105185.

[4] P. Astrahan, A. Lupu, E. Leibovici, S. Ninio, BTEX and PAH contributions to Lake Kinneret water: a seasonal-based study of volatile and semi-volatile anthropogenic pollutants in freshwater sources, Environ. Sci. Pollut. Res. 30 (21) (May 2023) 61145–61159, https://doi.org/10.1007/s11356-023-26724-9.

[5] M. Dehghani, A. Mohammadpour, A. Abbasi, I. Rostami, E. Gharehchahi, Z. Derakhshan, M. Ferrante, G.O. Conti, Health risks of inhalation exposure to BTEX in a municipal wastewater treatment plant in Middle East city: Shiraz, Iran, Environ. Res. 204 (Mar. 2022) 112155, https://doi.org/10.1016/j.envres.2021.112155.

[6] A. Mustafa, M.K. Azim, Z. Raza, J.A. Kori, BTEX removal in a modified free water surface wetland, Chem. Eng. J. 333 (Feb. 2018) 451–455, https://doi.org/10.1016/j.cej.2017.09.168.

[7] C.F. Bustillo-Lecompte, D. Kakar, M. Mehrvar, Photochemical treatment of benzene, toluene, ethylbenzene, and xylenes (BTEX) in aqueous solutions using advanced oxidation processes: towards a cleaner production in the petroleum refining and petrochemical industries, J. Clean. Prod. 186 (June 2018) 609–617, https://doi.org/10.1016/j.jclepro.2018.03.135.

[8] O. Fayemiwo, K. Moothi, M. Daramola, BTEX compounds in water – future trends and directions for water treatment, Water SA 43 (4) (Oct. 2017) 602–613, https://doi.org/10.4314/wsa.v43i4.08.

[9] N. Enemuo, H. Richards, M.O. Daramola, Preparation of hydrophilic PVDF membrane via blending with Fe3O4 nanoparticles and PVA for improved membrane performance in BTEX removal from wastewater, J. Environ. Chem. Eng. 13 (3) (June 2025) 116135, https://doi.org/10.1016/j.jece.2025.116135.

[10] D. Gupta, A. Boora, A. Thakur, T.K. Gupta, Green and sustainable synthesis of nanomaterials: recent advancements and limitations, Environ. Res. 231 (Aug. 2023) 116316, https://doi.org/10.1016/j.envres.2023.116316.

[11] R.A. Banjara, A. Kumar, R.K. Aneshwari, M.L. Satnami, S.K. Sinha, A comparative analysis of chemical vs green synthesis of nanoparticles and their various applications, Environ. Nanotechnol. Monit. Manag. 22 (Dec. 2024) 100988, https://doi.org/10.1016/j.enmm.2024.100988.

[12] M. Pradeep, D. Kruszka, P. Kachlicki, D. Mondal, G. Franklin, Uncovering the phytochemical basis and the mechanism of plant extract-mediated eco-friendly synthesis of silver nanoparticles using ultra-performance liquid chromatography coupled with a photodiode array and high-resolution mass spectrometry, ACS Sustain. Chem. Eng. 10 (1) (Jan. 2022) 562–571, https://doi.org/10.1021/acssuschemeng.1c06960.

[13] M. Teimouri, F. Khosravi-Nejad, F. Attar, A.A. Saboury, I. Kostova, G. Benelli, M. Falahati, Gold nanoparticles fabrication by plant extracts: synthesis, characterization, degradation of 4-nitrophenol from industrial wastewater, and insecticidal activity – A review', J. Clean. Prod. 184 (May 2018) 740–753, https://doi.org/10.1016/j.jclepro.2018.02.268.

[14] G.T. Tran, N.T.H. Nguyen, N.T.T. Nguyen, T.T.T. Nguyen, D.T.C. Nguyen, T.V. Tran, Plant extract-mediated synthesis of aluminum oxide nanoparticles for water treatment and biomedical applications: a review, Environ. Chem. Lett. 21 (4) (Aug. 2023) 2417–2439, https://doi.org/10.1007/s10311-023-01607-0.

[15] L. Liu, C. Yu, S. Ahmad, C. Ri, J. Tang, Preferential role of distinct phytochemicals in biosynthesis and antibacterial activity of silver nanoparticles, J. Environ. Manage. 344 (Oct. 2023) 118546, https://doi.org/10.1016/j.jenvman.2023.118546.

[16] D.A. Bopape, D.E. Motaung, N.C. Hintsho-Mbita, Green synthesis of ZnO: effect of plant concentration on the morphology, optical properties and photodegradation of dyes and antibiotics in wastewater, Optik (Stuttg) 251 (Feb. 2022) 168459, https://doi.org/10.1016/j.ijleo.2021.168459.

[17] S. Wu, L. Tian, Diverse phytochemicals and bioactivities in the ancient fruit and modern functional food pomegranate (Punica granatum), Molecules 22 (10) (Oct. 2017) 10, https://doi.org/10.3390/molecules22101606. Art. no.

[18] B. Singh, J.P. Singh, A. Kaur, N. Singh, Phenolic compounds as beneficial phytochemicals in pomegranate (*Punica granatum* L.) peel: A review, Food Chem 261 (Sept. 2018) 75–86, https://doi.org/10.1016/j.foodchem.2018.04.039.

[19] T. Volschenk, Water use and irrigation management of pomegranate trees - A review, Agric. Water Manag. 241 (Nov. 2020) 106375, https://doi.org/10.1016/j.agwat.2020.106375.

[20] V.L. Singleton, J.A. Rossi, Colorimetry of total phenolics with phosphomolybdic-phosphotungstic acid reagents, Am. J. Enol. Vitic. 16 (3) (Jan. 1965) 144–158, https://doi.org/10.5344/ajev.1965.16.3.144.

[21] V. Kumar, S. Singh, B. Srivastava, R. Bhadouria, R. Singh, Green synthesis of silver nanoparticles using leaf extract of Holoptelea integrifolia and preliminary investigation of its antioxidant, anti-inflammatory, antidiabetic and antibacterial activities, J. Environ. Chem. Eng. 7 (3) (June 2019) 103094, https://doi.org/10.1016/j.jece.2019.103094.

[22] R.M. Cornell, U. Schwertmann, The Iron Oxides: Structure, Properties, Reactions, Occurrences and Uses, John Wiley & Sons, 2003.

[23] A.B.D. Nandiyanto, R. Oktiani, R. Ragadhita, How to read and interpret FTIR spectroscope of organic material, Indones. J. Sci. Technol. 4 (1) (2019) 1. Art. no.
[24] X. Jin, Y. Liu, J. Tan, G. Owens, Z. Chen, Removal of Cr(VI) from aqueous solutions via reduction and absorption by green synthesized iron nanoparticles, J. Clean. Prod. 176 (Mar. 2018) 929–936, https://doi.org/10.1016/j.jclepro.2017.12.026.
[25] N. Saha, S. Dutta Gupta, Low-dose toxicity of biogenic silver nanoparticles fabricated by *Swertia chirata* on root tips and flower buds of *Allium cepa*, J. Hazard. Mater. 330 (May 2017) 18–28, https://doi.org/10.1016/j.jhazmat.2017.01.021.
[26] W. Shen, Y. Qu, X. Pei, S. Li, S. You, J. Wang, Z. Zhang, J. Zhou, Catalytic reduction of 4-nitrophenol using gold nanoparticles biosynthesized by cell-free extracts of *Aspergillus* sp. WL-Au, J. Hazard. Mater. 321 (Jan. 2017) 299–306, https://doi.org/10.1016/j.jhazmat.2016.07.051.
[27] F. Luo, D. Yang, Z. Chen, M. Megharaj, R. Naidu, One-step green synthesis of bimetallic Fe/Pd nanoparticles used to degrade Orange II, J. Hazard. Mater. 303 (Feb. 2016) 145–153, https://doi.org/10.1016/j.jhazmat.2015.10.034.
[28] M. Stan, M-L. Soran, C. Leostean, A. Popa, M. Stefan, M.D. Lazar, O. Opris, T-D Silipas, A.S. Porav, Removal of antibiotics from aqueous solutions by green synthesized magnetite nanoparticles with selected agro-waste extracts, Process Saf. Environ. Prot. 107 (Apr. 2017) 357–372, https://doi.org/10.1016/j.psep.2017.03.003.
[29] X. Liang, W. Feng, D. Liang, Y. Xu, X. Qiu, Hydroxyl/amino and Fe(III) co-grafted graphite carbon nitride for photocatalytic removal of volatile organic compounds, Environ. Res. 197 (June 2021) 111044, https://doi.org/10.1016/j.envres.2021.111044.
[30] D. Patiño-Ruiz, L. Sánchez-Botero, L. Tejeda-Benitez, J. Hinestroza, A. Herrera, Green synthesis of iron oxide nanoparticles using *Cymbopogon citratus* extract and sodium carbonate salt: nanotoxicological considerations for potential environmental applications, Environ. Nanotechnol. Monit. Manag. 14 (Dec. 2020) 100377, https://doi.org/10.1016/j.enmm.2020.100377.
[31] K. Pyrzynska, A. Sentkowska, Biosynthesis of selenium nanoparticles using plant extracts, J. Nanostructure Chem. 12 (4) (Aug. 2022) 467–480, https://doi.org/10.1007/s40097-021-00435-4.
[32] S. Ying, Z. Guan, P.C. Ofoegbu, P. Clubb, C. Rico, F. He, J. Hong, Green synthesis of nanoparticles: current developments and limitations, Environ. Technol. Innov. 26 (May 2022) 102336, https://doi.org/10.1016/j.eti.2022.102336.
[33] Z. Wu, D. Zhao, Ordered mesoporous materials as adsorbents, Chem. Commun. 47 (12) (2011) 3332–3338, https://doi.org/10.1039/C0CC04909C.
[34] J. Wang, Q. Ma, Y. Wang, Z. Li, Z. Li, Q. Yuan, New insights into the structure–performance relationships of mesoporous materials in analytical science, Chem. Soc. Rev. 47 (23) (2018) 8766–8803, https://doi.org/10.1039/C8CS00658J.
[35] S.P. Yeap, J. Lim, B.S. Ooi, A.L. Ahmad, Feasibility of electrostatic-mediated *post*-functionalization to induce long term colloidal stability and stability after freeze drying of amphoteric nanoparticles, Colloid Interface Sci. Commun. 23 (Mar. 2018) 14–20, https://doi.org/10.1016/j.colcom.2018.02.003.
[36] N. Wang, C. Hsu, L. Zhu, S. Tseng, J.-P. Hsu, Influence of metal oxide nanoparticles concentration on their zeta potential, J. Colloid Interface Sci. 407 (Oct. 2013) 22–28, https://doi.org/10.1016/j.jcis.2013.05.058.
[37] D.C.C.da S. Medeiros, P. Chelme-Ayala, C. Benally, B.S. Al-Anzi, M. Gamal El-Din, Review on carbon-based adsorbents from organic feedstocks for removal of organic contaminants from oil and gas industry process water: production, adsorption performance and research gaps, J. Environ. Manage. 320 (Oct. 2022) 115739, https://doi.org/10.1016/j.jenvman.2022.115739.
[38] M. Masuku, L. Ouma, A. Pholosi, Microwave assisted synthesis of oleic acid modified magnetite nanoparticles for benzene adsorption, Environ. Nanotechnol. Monit. Manag. 15 (May 2021) 100429, https://doi.org/10.1016/j.enmm.2021.100429.
[39] C.Z. Ye, P.A. Ariya, Co-adsorption of gaseous benzene, toluene, ethylbenzene, m-xylene (BTEX) and SO_2 on recyclable Fe_3O_4 nanoparticles at 0–101% relative humidities, J. Environ. Sci. 31 (May 2015) 164–174, https://doi.org/10.1016/j.jes.2014.10.019.
[40] X. Guo, J. Wang, A general kinetic model for adsorption: theoretical analysis and modeling, J. Mol. Liq. 288 (Aug. 2019) 111100, https://doi.org/10.1016/j.molliq.2019.111100.
[41] M.A. Al-Ghouti, D.A. Da'ana, Guidelines for the use and interpretation of adsorption isotherm models: A review, J. Hazard. Mater. 393 (July 2020) 122383, https://doi.org/10.1016/j.jhazmat.2020.122383.
[42] A.S. Mahmoud, M.K. Mostafa, S.A. Abdel-Gawad, Artificial intelligence for the removal of benzene, toluene, ethyl benzene and xylene (BTEX) from aqueous solutions using iron nanoparticles, Water Supply 18 (5) (Nov. 2017) 1650–1663, https://doi.org/10.2166/ws.2017.225.
[43] H.I. Eldos, M. Khan, N. Zouari, S. Saeed, M.A. Al-Ghouti, Adsorptive removal of volatile petroleum hydrocarbons from aqueous solution by zeolite imidazole framework (ZIF-8) and iron oxide (Fe3O4) nanoparticles, Environ. Technol. Innov. 32 (Nov. 2023) 103382, https://doi.org/10.1016/j.eti.2023.103382.
[44] N.Y. Dzade, A. Roldan, N.H. De Leeuw, A density functional theory study of the adsorption of benzene on hematite (α-Fe2O3) surfaces, Minerals 4 (1) (Mar. 2014) 1, https://doi.org/10.3390/min4010089. Art. no.
[45] S. Nakamura, Y. Tsuji, K. Yoshizawa, Role of hydrogen-bonding and OH−π interactions in the adhesion of epoxy resin on hydrophilic surfaces, ACS Omega 5 (40) (Oct. 2020) 26211–26219, https://doi.org/10.1021/acsomega.0c03798.
[46] C. Di Mino, A.G. Seel, A.J. Clancy, T.F. Headen, T. Földes, E. Rosta, A. Sella, N.T. Skipper, Strong structuring arising from weak cooperative O-H···π and C-H···O hydrogen bonding in benzene-methanol solution, Nat. Commun. 14 (1) (Sept. 2023) 1, https://doi.org/10.1038/s41467-023-41451-y. Art. no.